FINAL REPORT

Underwater Munitions Expert System to Predict Mobility and Burial

SERDP Project MR-2227

NOVEMBER 2017

Sarah Rennie
Johns Hopkins Applied Physics Laboratory

Distribution Statement A
This document has been cleared for public release

SERDP
DOD ▪ EPA ▪ DOE

Page Intentionally Left Blank

REPORT DOCUMENTATION PAGE

Form Approved
OMB No. 0704-0188

The public reporting burden for this collection of information is estimated to average 1 hour per response, including the time for reviewing instructions, searching existing data sources, gathering and maintaining the data needed, and completing and reviewing the collection of information. Send comments regarding this burden estimate or any other aspect of this collection of information, including suggestions for reducing the burden, to Department of Defense, Washington Headquarters Services, Directorate for Information Operations and Reports (0704-0188), 1215 Jefferson Davis Highway, Suite 1204, Arlington, VA 22202-4302. Respondents should be aware that notwithstanding any other provision of law, no person shall be subject to any penalty for failing to comply with a collection of information if it does not display a currently valid OMB control number.
PLEASE DO NOT RETURN YOUR FORM TO THE ABOVE ADDRESS.

1. REPORT DATE *(DD-MM-YYYY)*	2. REPORT TYPE	3. DATES COVERED *(From - To)*
11/14/2017	Final Report	9/28/2012 - 3/30/2016

4. TITLE AND SUBTITLE
Underwater Munitions Expert System to Predict Mobility and Burial

5a. CONTRACT NUMBER
Contract: 12-C-0032

5b. GRANT NUMBER

5c. PROGRAM ELEMENT NUMBER

6. AUTHOR(S)
Sarah Rennie

5d. PROJECT NUMBER
MR-2227

5e. TASK NUMBER

5f. WORK UNIT NUMBER

7. PERFORMING ORGANIZATION NAME(S) AND ADDRESS(ES)
Johns Hopkins
11100 Johns Hopkins Rd.
Laurel, MD 20723

8. PERFORMING ORGANIZATION REPORT NUMBER
MR-2227

9. SPONSORING/MONITORING AGENCY NAME(S) AND ADDRESS(ES)
Strategic Environmental Research and Development Program
4800 Mark Center Drive, Suite 17D03
Alexandria, VA 22350-3605

10. SPONSOR/MONITOR'S ACRONYM(S)
SERDP

11. SPONSOR/MONITOR'S REPORT NUMBER(S)
MR-2227

12. DISTRIBUTION/AVAILABILITY STATEMENT
Distrubution A: open to public release

13. SUPPLEMENTARY NOTES

14. ABSTRACT
A computer-based probabilistic expert system to predict mobility and burial of underwater munitions is under development. This Underwater Munitions Expert System (UnMES) will help guide remediation management of underwater sites contaminated with abandoned munitions. This report documents the progress made in the development of UnMES during the Project MR-2227 contract period (2013-2016). The objective of this project is to build a demonstration computer tool implementing a probabilistic system that will predict patterns of migration, exposure and aggregation for underwater munitions.

15. SUBJECT TERMS
Underwater Munitions, Mobility, Burial, Application Programmer Interface, Graphical Information System, Munitions and Explosives of Concern,

16. SECURITY CLASSIFICATION OF:			17. LIMITATION OF ABSTRACT	18. NUMBER OF PAGES	19a. NAME OF RESPONSIBLE PERSON
a. REPORT	b. ABSTRACT	c. THIS PAGE			Sarah Rennie
					19b. TELEPHONE NUMBER *(Include area code)*
UNCLASS	UNCLASS	UNCLASS	UNCLASS	65	443-778-8178

Page Intentionally Left Blank

This report was prepared under contract to the Department of Defense Strategic Environmental Research and Development Program (SERDP). The publication of this report does not indicate endorsement by the Department of Defense, nor should the contents be construed as reflecting the official policy or position of the Department of Defense. Reference herein to any specific commercial product, process, or service by trade name, trademark, manufacturer, or otherwise, does not necessarily constitute or imply its endorsement, recommendation, or favoring by the Department of Defense.

Page Intentionally Left Blank

Underwater Munitions Expert System: Demonstration and Evaluation Report

Table of contents

Page #

Abstract 1

1. Introduction 2
   - 1.1 Objective 3
   - 1.2 Background 3
   - 1.3 Methods 4
2. UnMES Design Update 5
   - 2.1 UXO Scour Burial 6
   - 2.2 Influence of UXO Density 7
   - 2.3 Acceleration Effects | Oscillatory Flow under Waves 11
     - 2.3.1 Scour Burial Dependence on KC 11
     - 2.3.2 Bottom Friction under Currents and Waves 14
   - 2.4 Burial Dependence on Angle of Attack 16
   - 2.5 Inclusion of Inertial factor for Mobility Threshold 19
   - 2.6 Migration Distance 20
3. Prediction Performance Assessment 21
   - 3.1 Scour burial and mobility during TREX13 21
   - 3.2 Mobility at Long Point, Martha's Vineyard 24
   - 3.3 Probabilistic Performance 26
4. Spatial Domain Provincing 31
5. Summary and Implications 35

Literature Cited

Appendix A: MATLAB code for predicting burial and onset of mobility.

Appendix B: Rule of Thumb algorithms estimating fluidization & migration distance

Appendix C: Example Conditional Probability Table

Appendix D: List of Scientific and Technical Publications

Underwater Munitions Expert System: Demonstration and Evaluation Report

Acronyms

API – Application Programmer Interface
APL – Applied Physics Laboratory
BN – Bayesian Network
CERCLA – Comprehensive Environmental Response, Compensation, and Liability Act
CFD – Computational Fluid Dynamics
CPT – Conditional Probability Table(s)
DBDB-V – Digital Bathymetric Data Base, Variable resolution (DBDBV)
DERP – Defense Environmental Restoration Program
d_{sed} – Sediment grain size
EPA – Environmental Protection Agency
ESTCP – Environmental Security Technology Certification Program
FRF – Field Research Facility, USACE, Duck, North Carolina
GIS – Graphical Information System
GoM – Gulf of Mexico
H_{sig} – Significant wave height
h_{sigma} – Standard deviation of bathymetry about the mean (temporal)
JALBTCX – Joint Airborne Lidar Bathymetry Technical Center of Expertise
JHU – The Johns Hopkins University
MEC – Munitions and Explosives of Concern
MC – Monte Carlo
MR – Munitions Response
NAVFAC – Naval Facilities Engineering Command
NAVOCEANO – Naval Oceanographic Office
NCEP – National Centers for Environmental Prediction
NRL – Naval Research Laboratory
NWPS – Nearshore Wave Prediction System
ONR – Office of Naval Research
PDF – Probability Distribution Function
PMF – Probability Mass Function
SERDP – Strategic Environmental Research and Development Program
S_g – Specific gravity
STWAVE – Steady State Spectral Wave Model
SWAN – Simulating WAves Nearshore, 3rd generation wave model
U_{bot} – Velocity of fluid flow at the bottom of the water column
UnMES – Underwater Munitions Expert System
USACE – United States Army Corps of Engineers
UXO – Unexploded Ordnance
WHOI – Woods Hole Oceanographic Institution

Underwater Munitions Expert System: Demonstration and Evaluation Report

Abstract

A computer-based probabilistic expert system to predict mobility and burial of underwater munitions is under development. This Underwater Munitions Expert System (UnMES) will help guide remediation management of underwater sites contaminated with abandoned munitions. This report documents the progress made in the development of UnMES during the Project MR-2227 contract period (2013-2016).

Objectives: A comprehensive model for predicting the location and possible burial of underwater munitions is required to advise site managers as they plan monitoring or clean-up activities. Because in any real-world scenario, the exact types and initial locations of the munitions as well as the environmental conditions will not be exactly known, a meaningful approach for predicting munitions' locations and burial extent will be probabilistic in nature. The objective of this project is to build a demonstration computer tool implementing a probabilistic system that will predict patterns of migration, exposure and aggregation for underwater munitions.

Technical Approach: In order to develop this expert system a number of hydrodynamic and geological processes must be understood and related to the interaction of munitions with the underlying sediments and the environmental forces. Simple models relating causal forces acting on the underwater munitions and the associated sediment responses have been developed to predict scour burial and motion initiation. Recent work has extended the models to account for additional factors that are particularly important under wave-driven conditions. These models are used in the construction of a probabilistic Bayesian network forming the core of UnMES.

Results: Implemented improvements to UnMES include models for: the role of munitions density on burial and migration; the effects of oscillatory flow; the effects of the angle of bottom flow; acceleration effects on initiation of motion by the incorporation of an inertial factor for mobility threshold; and preliminary modeling of migration distance. In addition, model predictions are compared to field data obtained during SERDP sponsored field tests to assess the skill of the both the underlying process models and the Bayesian Network

implementation of UnMES. The process models are assessed by deterministic time-series comparisons and traditional metrics such as the coefficient of correlation. The summary statistic for the comparisons of burial results was $r^2 = 0.78$, indicating that the model accounted for over ¾ of the observed burial behavior. The Bayesian Network was evaluated by comparison of field observation histograms with predicted probability distributions using a Ranked Probability Skill Score. The models and expert system predictions generally agreed with the observations, providing substantial guidance regarding the munitions behavior. The spread in the output distributions predicted by UnMES correctly captured the observed variability.

Benefits: This Demonstration Version of UnMES brings together in a coherent and organized manner current knowledge on the manner in which munitions on the seabed can bury or migrate. The probabilistic construct feeds naturally into risk-assessment models used by site managers for remedial investigation decisions. With the expert system guidance regarding the timing, location and operational choices for assessment surveys and subsequent clean-up, these efforts can be more efficiently planned and executed. Prediction of burial, which affects detection and classification performance by geophysical, acoustic and optical sensors, will guide optimal selection of sensor technologies. Knowledge of migration thresholds at remediation sites will allow evaluation of potential munitions relocation by storms of varying magnitudes. Additional benefit provided by the expert system is that it can function as a documented archive synthesizing records of laboratory and field research as well as databases of environmental conditions.

1. Introduction

Development of an Underwater Munitions Expert System was initiated under support of the United States Department of Defense Strategic Environmental Research and Development Program (SERDP), Project MR-2227 (2013-2016). The initial research focused on accumulating domain knowledge of the phenomena and understanding important physical processes relevant to UXO burial and migration, enhanced by focused laboratory experiments. A preliminary model framework was proposed [Rennie and Brandt, 2015] and shared with the munitions response research community to stimulate collaboration, essential for development of a practical expert system. Feedback from the research community emphasized a number of additional mechanisms and factors controlling the behavior of migration and burial, leading to a follow-on SERDP project, MR-2645 in 2016-2019. This report documents the progress made on the expert system through 2016.

1.1 Objective

The Munitions Response program of SERDP is focused on developing innovative methods to remediate and sustainably administer areas polluted by discarded munitions. Construction of the Underwater Munitions Expert System (UnMES) is aimed towards providing a computer-based decision support tool for management of aquatic sites requiring remediation. The UnMES is a probabilistic Bayesian expert system which synthesizes databases of environmental conditions and recent research into physics-based process modeling of munitions' behavior in response to environmental forcing, with the goal of predicting the location of munitions and their degree of burial at underwater sites. As a result, UnMES will provide improved guidance for underwater munitions site assessment and remediation efforts.

1.2 Background

As a legacy of years of US military activities, including training and testing, there are numerous current and former Department of Defense (DoD) underwater sites contaminated with military munitions. These can range in size from bombs and mines down to small arms ammunition. These may be classified as unexploded ordnance (UXO) when they had been primed for action but remained unexploded due to malfunction, design or some other cause. Other munitions and explosives of concern (MEC) may have been abandoned without proper disposal (Discarded Military Munitions or DMM), and continue to pose a safety hazard. In this report, the term UXO is used to denote MEC of all types and sources. At many of these inland water and coastal areas, the risk of human interaction with UXO is of concern, and the contaminated site will be put under the Defense Environmental Restoration Program (DERP) whose actions follow the Comprehensive Environmental Response, Compensation, and Liability Act (CERCLA) response process.

Compared to terrestrial sites, underwater environments are subject to more dynamic conditions. Burial or excavation of the UXO by bottom currents driven by waves and tides can also cause mobility. The extent of the search area covered for a region containing underwater UXO is limited using present platform and sensor technology. Therefore, it is important to predict the fate of munitions, including areas of concentration and probability of exposure, in order to maximize the search and removal of underwater UXO.

1.3 Methods

The expert system is built on a Bayesian network, a useful tool to simulate natural systems in a probabilistic setting. The variables in a Bayesian network (BN) are represented by nodes, connected by arrows that symbolize dependent relationships. Each relationship is characterized by a conditional probability table (CPT) associated with the dependent node. A BN has a causal graphical structure that allows non-technical users to easily visualize the important factors and how they are interrelated. A common approach to building a BN network is to train the CPT using a dataset of example cases. Because the availability of field and laboratory data applicable to UXO burial and mobility is extremely limited, our approach has generally been to develop simple deterministic models that capture the first-order physics of the processes of interest. Then Monte Carlo simulations of these models are run over the relevant combinations of input variable in order to populate the CPTs in UnMES. For some nodes in the preliminary version of UnMES, where a validated deterministic model has not yet been developed, the CPT may be formed empirically using the data currently available (see for example Section 2.1, UXO density effects).

A BN represents the synthesis of current knowledge on the topic of interest. A preliminary design of UnMES was reported in Rennie and Brandt [2015] where a more complete introduction to Bayesian Networks is provided. As continuing research reveals new knowledge, additional nodes may be added to the network, or an existing CPT may be updated. To be consonant with the SERDP sponsored field tests that will be used for performance evaluation, the updated Demonstration version of UnMES, presented in this report, is focused on predicting conditions at coastal sites, where surface waves are the primary forcing. Relevant physics, in particular oscillatory effects, supplementary to that included in the preliminary version of UnMES [Rennie and Brandt, 2015] is presented in Section 2. A schematic for the Demonstration version of the UnMES BN is shown in Figure 1.1. In order to use the available field data for assessment, the Demonstration UnMES is designed to predict burial and migration behavior over relatively short time scales, e.g. a single storm event lasting a day or two. As such, the long time scale processes considered in the preliminary UnMES design, e.g. erosion, are not considered.

The BN is implemented in the software product Netica™ [Norsys, 2017] which can use data input and output connections from MATLAB code through a JAVA API. In addition to predicting outcome probabilities, the BN can provide insight on the sensitivity of predicted outcomes to changes in network variables and quantify which factors have the strongest

influence in various scenarios. This BN is designed to represent conditions at one location in the spatial domain (see Section 4).

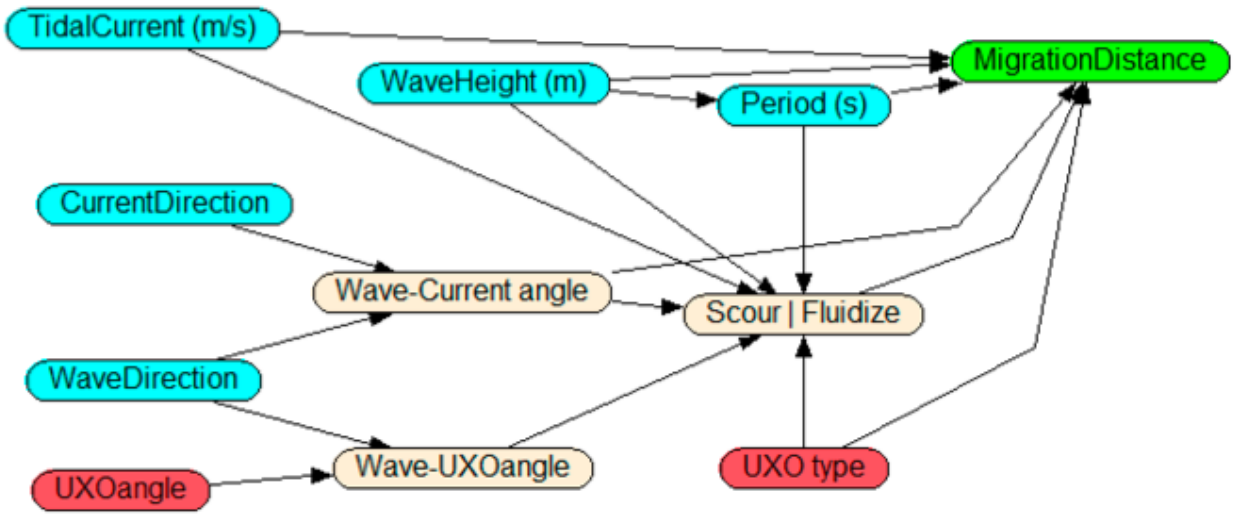

Figure 1.1 Schematic diagram of Bayesian Network which comprises the 2016 Demonstration version of UnMES incorporating additional physics based processes discussed in Section 2. Nodes in blue indicate environmental inputs, nodes in red describe UXO conditions. The green node outputs a migration distance distribution prediction.

UnMES would ultimately function as a component in a comprehensive Decision Support Tool (DST) that is used as part of structured decision-making for site remediation. A potential DST framework incorporating UnMES is outlined in Rennie and Brandt [2015]. Because site management naturally involves assessment of spatial variability, integration of the BN with a geographic information system (GIS) is desired to provide geographic coverage of inputs and map-based illustration of spatial patterns of predicted output. An initial implementation of UnMES in a spatial construct is documented in Section 4. Prediction performance of the updated UnMES algorithms is presented in Section 3.

2. UnMES Design Update

The initial design of UnMES [Rennie and Brandt, 2015] contained a preliminary version of the modeling approach used to implement burial mechanisms including the far-field effects of erosion or accretion whose conditional probabilities were derived from site-specific statistics, and the local effect of scour, for which a physics-based process model was used. The Demonstration UnMES focuses on local effects, including burial by fluidization. This

section presents updated modeling for burial processes based on our recent studies of these processes [Friedrichs *et al*., 2016; Rennie *et al*., 2017].

2.1 UXO Scour Burial

Scour occurs when the presence of an object on a non-cohesive granular bed causes local acceleration of the near-bed flow promoting the mobilization of sediment around the object. This enhanced erosion causes a scour pit to develop in which the object buries.

The model used in the preliminary version of UnMES predicted equilibrium scour burial based only on the sediment Shields parameter, θ, the ratio between the fluid force (bottom shear stress) and the weight of the sediment particles, defined as

$$\theta = \frac{\frac{1}{2} f_\tau U^2}{g\,(S_{sed}-1) d_{sed}}, \tag{2.1}$$

where U is the bottom current velocity, f_τ the friction coefficient, g gravitational acceleration, $S_{sed} = \rho_s/\rho_w$, with ρ_s the sediment grain density, ρ_w the water density, and d_{sed} the median sand grain size. Fractional burial depth (i.e. the ratio of the object burial depth, B to its diameter, D) under steady currents has a relationship with θ best represented by the equation

$$B/D = \boldsymbol{a}\,\theta^{\boldsymbol{b}}. \tag{2.2}$$

As no accounting for the UXO size or shape is represented in the sediment Shields parameterization, Rennie *et al.* [2017] proposed the use of different empirical coefficients ***a*** and ***b*** to account for the varying behavior in laboratory experiments for UXO of different shapes and sizes. The choice of coefficients is dependent on the method used to estimate the friction factor f_τ; the formulae used in the updated demonstration UnMES are documented in Section 2.3.2. In addition, burial prediction by Equation 2.2 neglects the density of the UXO, which is considered in Section 2.2.

For application of UnMES to coastal sites where surface waves are the primary forcing mechanism for UXO burial and mobility, a modified process model is required. Friedrichs *et al.* [2016] reviewed the extensive body of literature investigating scour-induced burial, taking full advantage of the contributions from Marcelo Garcia's laboratory [e.g. Cataño-Lopera & Garcia, 2007], and determined that under wave-dominated conditions burial is significantly influenced by several factors addition to θ, including inertia of oscillatory flow, and the angle between the orbital velocity and the UXO main axis. The practical application of these results within the probabilistic framework of UnMES is discussed in Section 2.3.

For wave-driven flows, the Keulegan-Carpenter number (KC) is a useful parameterization describing the importance of drag forces over inertial forces in oscillatory motion. KC is defined as

$$KC = U_m T/D \tag{2.3}$$

where U_m is maximum near-bed wave velocity, T is wave period, and D is object diameter. A modification to both the scour burial and migration nodes in UnMES to encompass the KC effect is included in Sections 2.3 and 2.5.

The role of the UXO density, ρ_{UXO} is not accounted for in either the θ or KC parameterizations, but is considered in several studies of scour burial [e.g. Cataño-Lopera *et al*. 2007]. Voropayev *et al.* [2003] ignores ρ_{UXO}, after assuming the UXO is sufficiently heavy so that it will not be mobilized. This assumption does not hold true in several of the SERDP supported field experiments where onset of mobility was part of the observation plan. Further consideration of the role of ρ_{UXO} in burial processes is the topic of Section 2.2. Consideration of UXO density and inertial effects will be included in the Demonstration version of UnMES evaluated in Section 5.

2.2 Influence of UXO Density

In the preliminary UnMES design, the munition density, ρ_{UXO} is an important factor in mobility, but not included in the burial nodes. The process of UXO burial in non-cohesive sediments was modeled using the sediment Shields parameter, where the degree of burial is quantified as B/D, with B = depth of burial and D is the diameter of the UXO. The scour mechanism was assumed to result in a maximum B/D of 1.2 [Whitehouse, 1998] because after the object is fully buried, it no longer causes local acceleration of the nearby sediment. Some studies (Cataño-Lopera and Garcıa, 2006), reported observations showing that denser objects buried deeper, however this effect was not quantified. Upon review of additional wave-driven studies, Friedrichs *et al.* [2016] reconsidered both the role of oscillatory flow (see Section 2.3) as well as the importance of ρ_{UXO} in influencing the depth of burial. For the range of experimental data reviewed, which was limited to lower energy conditions and larger cylinders, a very small influence was found for ρ_{UXO} on B/D. Note that the data considered was assembled from experiments specifically designed to study scour, and did not include any very high velocity flows where the role of object density may be more important; the maximum θ was less than 0.7 in the laboratory data considered in Friedrichs *et al.* [2016]. These data plotted in Figure 2.1 with blue "x", do not show any significant trend in burial due to density effects, illustrating why, for the lower energy regime, ρ_{UXO} was not included as a factor in predicting B/D.

With highly energetic near-bed flow, such as driven by strong storm waves, sediment transport at the sediment-water interface takes place as a "sheet flow" layer [Sumer *et al.,* 1996]. We use the term fluidization to refer the burial mechanism in this regime where bottom current forcing is strong enough to mobilize the entire seabed to some significant depth. This is distinguished from the mechanism termed liquefaction where a cycling pressure gradient drives fluctuations in pore pressure, resulting in bed instability [Foster *et al*., 2006]. In this high-energy regime with the upper layers of the sediment mobilized, any bedforms become washed out. The threshold for sheet flow is delimited by a minimum sediment Shields parameter value θ larger than 0.7 to 0.8 [Cataño-Lopera *et al*., 2007]. For sheet flow to include sediment in suspension, the threshold is $\theta > 0.9$ or 1.0 [Sumer *et al*., 1996]. For a bed composed of medium sand, this requires a minimum near-bed flow speed of just over 1 m/s. For the Demonstration UnMES, a threshold of θ larger than 0.7 was used to indicate fluidization conditions (see Appendix A and B).

Cataño-Lopera and García [2006] observed that heavy cylinders buried deeper in high-energy conditions. Similar to the behavior under liquefaction [Sumer, 2014] it is proposed that during bed fluidization UXO will sink when ρ_{UXO} is larger than some critical value of sediment density (ρ_{SED_CRIT}) at the water-sediment interface. Following the approach of liquefaction analyses, one estimate for ρ_{SED_CRIT} is the bulk density of wet sand, or a specific gravity, S_g = 2.0. Alternatively, results from both Cataño-Lopera *et al*. [2007] and Fahnestock and Haushild [1962] point to ρ_{SED_CRIT} equal the sediment grain density (S_g = 2.65), which may indicate that granular sorting is the dominant mechanism. During bed fluidization, Cataño-Lopera *et al*. [2007] observed very different behaviors based on ρ_{UXO}: the extremely dense (ρ_{UXO} = 7.9 g/cm^3) steel object sank rapidly into the bed and was buried within seconds, while lighter cylinders (ρ_{UXO} = 2.7 g/cm^3) did not bury, but moved horizontally with the flow. For the heavy cylinder, with relative density, $\rho_{UXO}/\rho_{SED_CRIT}$ = 7.9/2.65 = 3, B/D was observed to be 1.5. In a laboratory experiment reported by Calantoni [2016] the role of density was tested by generating sheet flow conditions in a tank where small cylindrical munitions of varying density had been placed on "sediment" composed of nylon beads with ρ_{SED_CRIT} = 1.15. These laboratory burial observations under sheet flow conditions are plotted in Figure 2.1 as solid triangles, and show an increase in burial fraction with relative UXO density, with an observed maximum close to B/D = 2.

Also plotted on Figure 2.1 are burial measurements from two SERDP field experiments during high-energy wave forcing (open symbols). Compared to the controlled laboratory experiments, in the field a complex mix of processes may be occurring at any one time. Burial data from the SERDP field experiment at Martha's Vineyard [Traykovski and Austin, 2017], were screened for conditions where the estimated θ was greater than 0.7 and these

higher energy burial observations are shown on Figure 2.1 as black circles. These observations only cover a small range of relative density, but there is a slight indication of increased burial with UXO density.

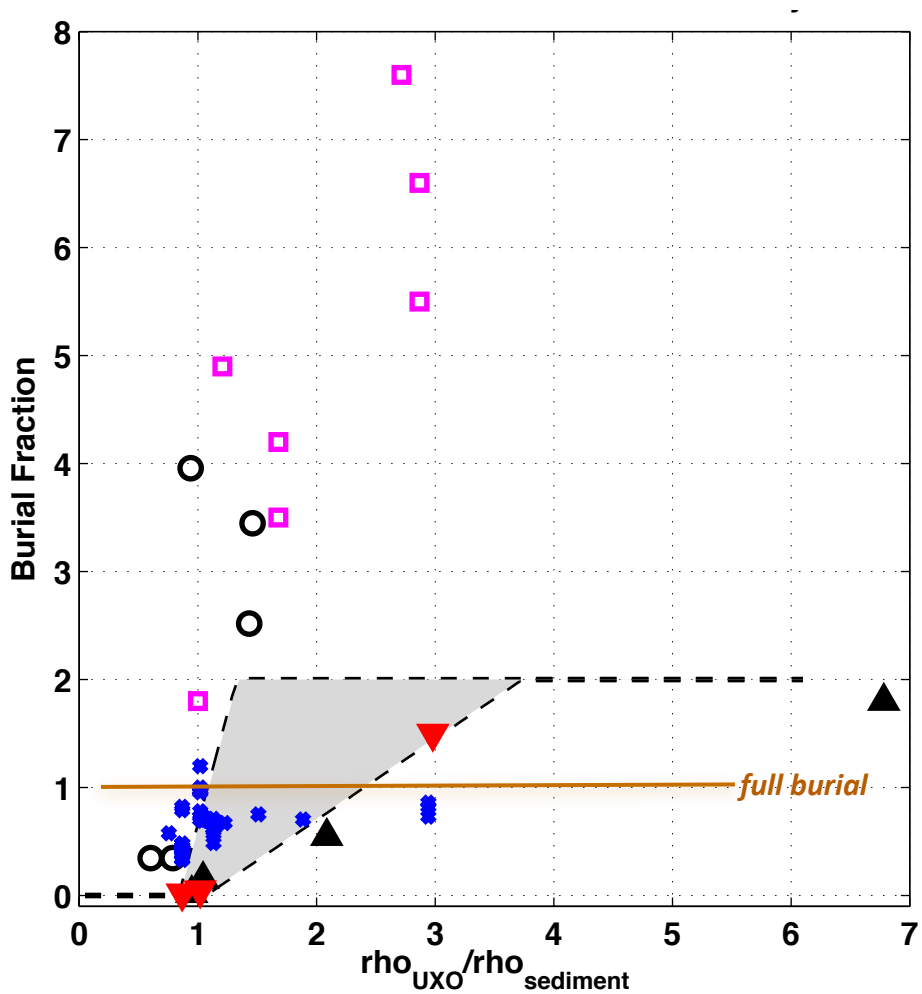

Figure 2.1 Burial fraction versus relative UXO density. Solid triangles from laboratory experiments with sheet flow conditions: red triangles = Cataño-Lopera *et al.* [2007], black triangles = Calantoni [2016]. Blue x shows relative density range included in Friedrichs *et al.* [2016] for lower energy scour. Open symbols from SERDP field experiments following high-energy conditions: black circle = Traykovski and Austin [2017], magenta squares = Calantoni [2016]. The grey shaded area indicates the region over which fluidization burial is predicted in a probabilistic manner.

Additional data from SERDP DUCK15 field test at Duck, NC [Calantoni, 2016], shown as magenta boxes in Figure 2.1, cover a wider range of UXO density. During DUCK15, the surrogate UXO deployed in 8 m water depth were subjected to a storm with significant wave height (H_{sig}) over 4m, with long period (T > 13 seconds) that resulted in near-bed flows of close to 1.5 m/s, creating fluidization conditions ($\theta > \sim 1$). While the DUCK15

exhibit a clear trend of increasing B/D with larger UXO density, it is difficult to interpret the magnitude of burial fraction as due solely to fluidization processes. The largest burial observed, with B/D ~ 7.6, represents an 81 mm mortar buried to a depth of over 0.6 m, which is much deeper than any sheet layer thickness envisioned. The large burial observations more likely represent interaction (possibly repeated) of fluidization with additional burial mechanisms including forced granular sorting (discussed below), and also the migration of bedforms such as ripples and sand waves [Voropayev *et al*. 1999].

Motivated by his laboratory and DUCK15 data, Calantoni [2016] proposed that for extreme hydrodynamic conditions, burial was dominated by granular sorting physics, with ρ_{UXO} as the dominant influence. There is an extensive research literature on particle sorting during movement, particularly from the mining geology field, which often focus as much on particle dimension as on density. Patterns of granular sorting behavior can be very complex, even paradoxical, as in the ubiquitous "brazil-nut effect" where a large particle rises to the top, even when the larger particle is denser than the smaller ones [Rosato *et al.,* 1987]. This phenomenon is generally attributed to the ability of smaller grains to filter down through the interstices between larger ones, so that with each jostling, the large particle is ratcheted upwards, even when it is significantly denser [Clement *et al.,* 2010]. During bedload transport, this can result in the inverse grading frequently seen in debris flows, or in the sediment of river beds [Viparelli *et al*., 2015]. What role various granular sorting phenomena play in the burial of UXO is not yet understood and requires further research.

For the present Demonstration version of UnMES, a simple fluidization model based on an *ad hoc* probabilistic relationship dependent on a relative density factor will be incorporated into the burial node labeled "Scour | Fluidize" in Figure 1.1. The relationship is guided by currently available relevant data discussed above, with burial depth assumed to stochastically lie within the grey shaded region in Figure 2.1. The conditional probability table will be formed by uniform draws from that region above the given UXO relative density, which is defined as the UXO density divided by the sand grain density, (nominally 2650 g/cm^3). The region for $\rho_{UXO}/\rho_{SED_CRIT} < 1$ corresponds to no burial, B/D ~ 0. There is a rapid transition to full burial for $\rho_{UXO}/\rho_{SED_CRIT}$ between 1 and 2.5. The role of time-varying pressure-gradient forces in causing fluidization is under investigation by two active SERDP projects, MR-2647 (Friedrichs) and MR-2731 (Foster). Results from their research will improve the fluidization burial model used in the next version of UnMES.

Note that the majority of munitions of interest have a density equal or greater than sand grain density (S_g > =2.65), e.g. Jenkins *et al.* [2013]. The exceptions include incendiary or

pyrotechnic munitions [OSPAR, 2013] and some missiles. A thorough inventory of size, shapes and densities for munitions of concern for remediation is being undertaken by Calantoni [2016].

2.3 Acceleration Effects | Oscillatory Flow under Waves

The model to predict scour burial as proposed in Rennie & Brandt [2015] was guided by laboratory experiments with steady currents [Rennie & Brandt, 2014] and did not include the effect of oscillatory flow. In wave-dominated environments, acceleration effects are important and must be included in the prediction of both scour and onset of mobility.

The maximum orbital excursion distance, A, under a wave is given by $A = U_m T/(2\pi)$, and represents the distance that sediment particles could be swept by wave motion. The Keulegan-Carpenter number (KC) as defined in Equation 2.3, is proportional to A, so it effectively represents the scale of vortices shed by oscillatory flow over the object resting on the bottom [Sumer and Fredsøe, 1990]. Therefore, the scour pit becomes larger with larger KC and burial is increased.

The model to predict onset of motion used in the preliminary version of UnMES [Rennie & Brandt, 2015] also focused on motion under steady (or slowly increasing) currents, with the force balance dominated by drag and friction. When considering the hydrodynamic forces exerted by waves, the additional inertia term is parameterized as an inverse function of KC [Sarpkaya, 1986]. For onset of motion, a smaller KC number indicates increased effective mobilizing force, as discussed in Rennie *et al*. [2017].

2.3.1 Scour Burial Dependence on KC

The scour process model in the Demonstration version on UnMES has been extended to include dependence on both θ and KC for burial under waves as determined by Friedrichs *et al.* [2016]. Based on studies comprising several hundred data points where burial was studied under waves plus currents, or waves alone, the best fit power law relationship was determined to be

$$B/D = p_1 (KC)^{p_2} \tag{2.4}$$

with p_1 = 0.1 (0.09, 0.12) and p_2 = 0.51 (0.46, 0.56) for large UXO with cylindrical or spherical shapes (r^2 = 0.62). These coefficients are nearly identical to those reported by Sumer and Fredsøe [1990]. The values in parentheses represent the 95% confidence interval (C.I.) for the coefficients based on the fit. Note that these measurements were for

cases where the long axis of the UXO was approximately perpendicular to the wave direction; the effect of small angles is considered in Section 2.4. For field data where wave height was measured, the maximum near-bed orbital velocity U_w was estimated from H_{sig} (the largest 1/3 of the waves as represented by a Rayleigh distribution) assuming that it is the larger waves that cause scour.

The majority of the data examined by Friedrichs *et al*. [2016] were obtained under controlled laboratory conditions where wave-only or current-only forcing can be studied. Under realistic coastal conditions in the field, the bottom velocity acting on the UXO will be forced by a combination of waves plus currents. The value of U_m used to compute both the friction factor f_w (Section 2.3.2) and the Keulegan-Carpenter number KC (Equation 2.3) for combined waves and currents is computed as $U_m = (U_w^2 + U_c^2 + 2U_wU_c\,|\cos\beta|)^{1/2}$ where U_c is the near-bed current velocity and β is the angle between U_w and U_c.

When U_w and U_c are parallel (cos β =1), the steady current will act in opposition to the orbital velocity during half of the wave cycle, reducing the effectiveness of U_w. An empirically-determined multiplicative factor is proposed to account for the proportion of the currents that are parallel to the wave direction, in the form of

$$f(U_{c||}/U_m) = \exp[-1.1(U_{c||}/U_m)], \quad \text{where } U_{c||} = U_c\cos(\beta). \tag{2.5}$$

In many circumstances when applying the expert system in coastal conditions, UnMES will not have exact knowledge of either the magnitude or direction of U_c. so that this factor will need to be estimated from general knowledge of the local current patterns. For near-shore conditions, it is assumed to be highly probable that U_c is perpendicular to U_w, so that cos β = 0 and $f(U_{c||}/U_m)$ =1. During time periods when currents are stronger than waves, i.e. $U_{c||}/U_m > 0.5$, a scheme to transition to use of the equation for scour burial forced by steady currents (Equation 2.2) is appropriate.

After normalizing the B/D observations by f(KC), and $f(U_{c||}/U_m)$, the coefficients for the remaining dependence on the sediment Shields parameter θ (Equation 2.2) were determined empirically using least-squares fitting in power law form. As in Rennie *et al.* [2017], there was some indication that separate fits may be required for cylinders versus tapered UXO; however there was little data for tapered cylinders under waves (only 6 out of 344 observations) and the data was of poor quality. It was decided to combine the tapered and full cylinder data before empirically determining the best fit dependence on θ. The combined predictive model for scour burial under waves is then

$$B/D = (1.85\ \theta^{0.34})\ 0.1\ (KC)^{0.51} \exp(-1.1\ U_{cll}/U_m) \quad (2.6)$$

Again, this model assumes represents the predicted burial when the UXO is oriented nearly perpendicular to the flow. In Figure 2.2 observations are plotted against predictions for the data collected in Friedrichs *et al*. [2016] where the diameter was larger than 1". The green circles represent data for cylinders under wave-dominated conditions. The red triangles are observations under steady currents. The process model equations, which are summarized in Table 2.1, below, capture 78% of the observed variability in Friedrich *et al.,* [2016] burial data; however, it appears that the deeper burial under waves will be somewhat over predicted. Improvements to the scour burial model will continue to be investigated in our project MR-2645 and in the allied SERDP project MR-2647 "Parameterized Process Models for Underwater Munitions Expert System" [Friedrichs, 2016].

2.3.2 Bottom Friction under Currents and Waves

The proposed coefficients values for the burial models (Equations 2.2 and 2.6) dependence on θ are applicable only if an approach consistent with Friedrichs *et al*. [2016] is used to estimate the bed friction coefficient f_τ used in Equation 2.1. To wit, the frictional force that bottom flow exerts on the seabed is expressed in terms of bed shear-stress τ, with $\tau = ½\rho f_\tau U^2$. Multiple methods of computing f_τ have been published. The magnitude of τ is driven by the vertical gradient in flow velocity in the boundary layer near the seabed. Because the boundary layer under a steady current is much thicker (order meters) than an oscillatory boundary layer under waves (order centimeters), peak τ is much larger for waves with maximum near-bed orbital velocity U_w than under a current with an equivalent $U_c = U_w$ [Soulsby, 1997]. Therefore two different methods are used in UnMES to compute wave and current friction coefficients.

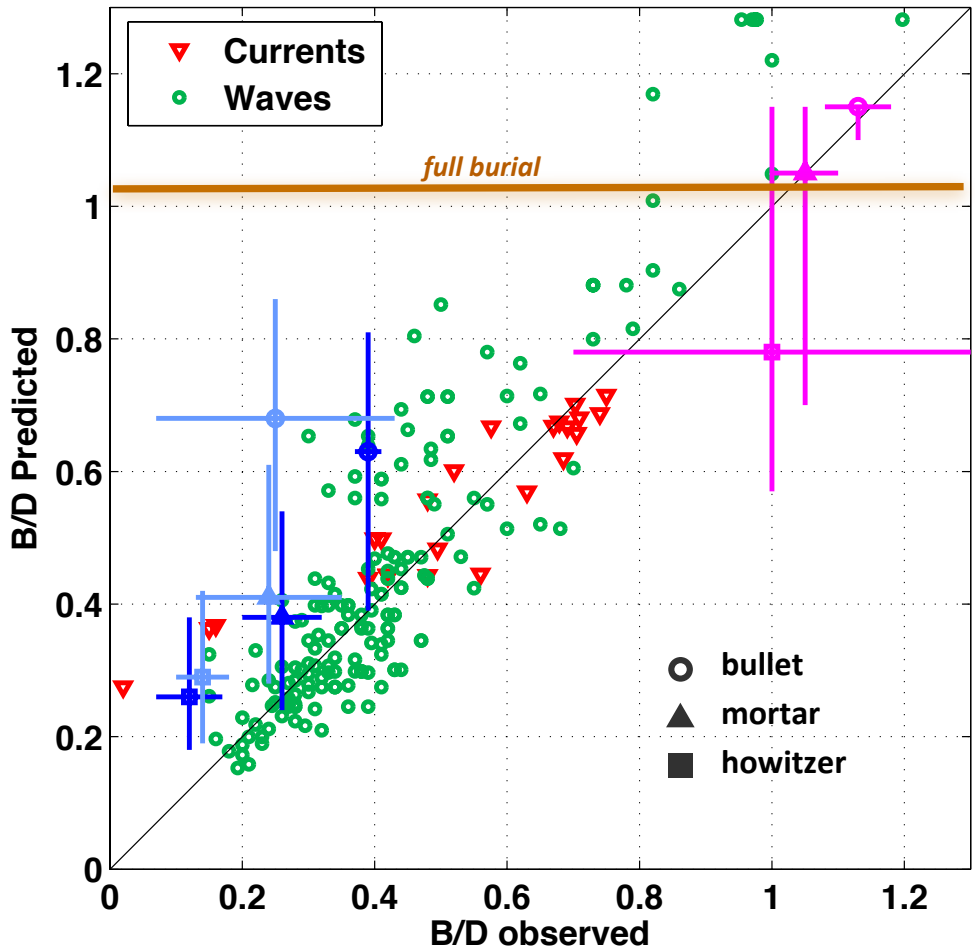

Figure 2.2 Comparison of scour burial data vs. predictions. Scatter points: laboratory data compiled from Friedrichs *et. al* [2016] with large diameter UXO under steady currents (red triangles) and under waves (green circles). Whiskers indicate observed and predicted burial for TREX13 field experiment with combined waves and currents (discussed in Section 3).

Boundary shear stress under a steady current is usually expressed in the form of a shear velocity $u_\star$ where $u_\star = (\tau/\rho)^{1/2}$. In Friedrichs *et al.* [2016], $u_\star$ is calculated from the observed current U_{obs} following Yalin [1992] as presented by Garcia [2008]. The relevant near-bed velocity U_c is computed by applying the law of the wall to adjust U_{obs} from its observed elevation to an elevation above the bed on the scale of the UXO diameter. Because the Yalin [1992] formulation is based on the roughness Reynolds number, which is itself a function of $u_\star$, an iterative method is used. Details of the computation are shown in Appendix A. Then the formula for the friction coefficient f_τ under currents is

$f_C = f_\tau = 2(u_*/U_c)^2$;. The results for f_C are plotted versus U_c in Figure 2.3 and can be seen to vary only slightly with current speed, but vary substantially with bottom roughness, estimated as a function of d_{sed}. Using this formulation, $\theta_C = \frac{\frac{1}{2} f_c U_C^2}{g\,(S_{sed}-1) d_{sed}}$ is the Shields parameter for currents.

Using this approach to compute the Shields parameter, Friedrichs *et al*. [2016] found the coefficients for Equation 2.2 to be ***a*** = 1.2 and ***b*** = 0.33 for large cylinders under steady currents when θ > 0.04 (higher bed shear stress, producing live bed scour). Tapered cylinders and small diameter (D ≤ 1") cylinders buried more easily; their burial fraction is represented by ***a*** = 13 and ***b*** = 1, i.e. B/D = 13θ during live-bed scour. During low bed shear stress under steady currents (clear water scour where θ < 0.04), the increase of B/D with θ is much steeper, with ***a*** ranging from 350 to 1200 and ***b*** between 2.1 to 2.4. The updated best-fit equations are summarized in Table 2.1 and are essentially the same as those published in Rennie *et al*. [2017], but somewhat different that the equations given in Rennie & Brandt [2015], largely due to adoption of the friction factor formula given above. Note that the magnitude of the "clear water" coefficients indicate that, in fine sands, scour burial to the depth of about half the diameter of the UXO is expected to occur under moderate bottom currents, e.g. U < 25 cm/s.

Using this method to compute f_W, the Shields number for waves is $\theta_W = \frac{\frac{1}{2} f_W U_W^2}{g\,(S_{sed}-1) d_{sed}}$ and burial can be estimated as a function of θ_W as shown in Table 2.1 where the empirical coefficients for different forcing conditions and UXO types are summarized. As mentioned in the previous section, the near-bed orbital velocity U_w is computed from the significant wave height H_{sig} using linear wave theory.

An error is noted in Rennie and Brandt [2014 and 2015] where scour burial under steady unidirectional currents was predicted as $\mathbf{a}\theta^{\mathbf{b}}$ using Shields numbers based on friction factors appropriate for waves. The corrected θ would be about half as small, resulting in a larger coefficient **a**.

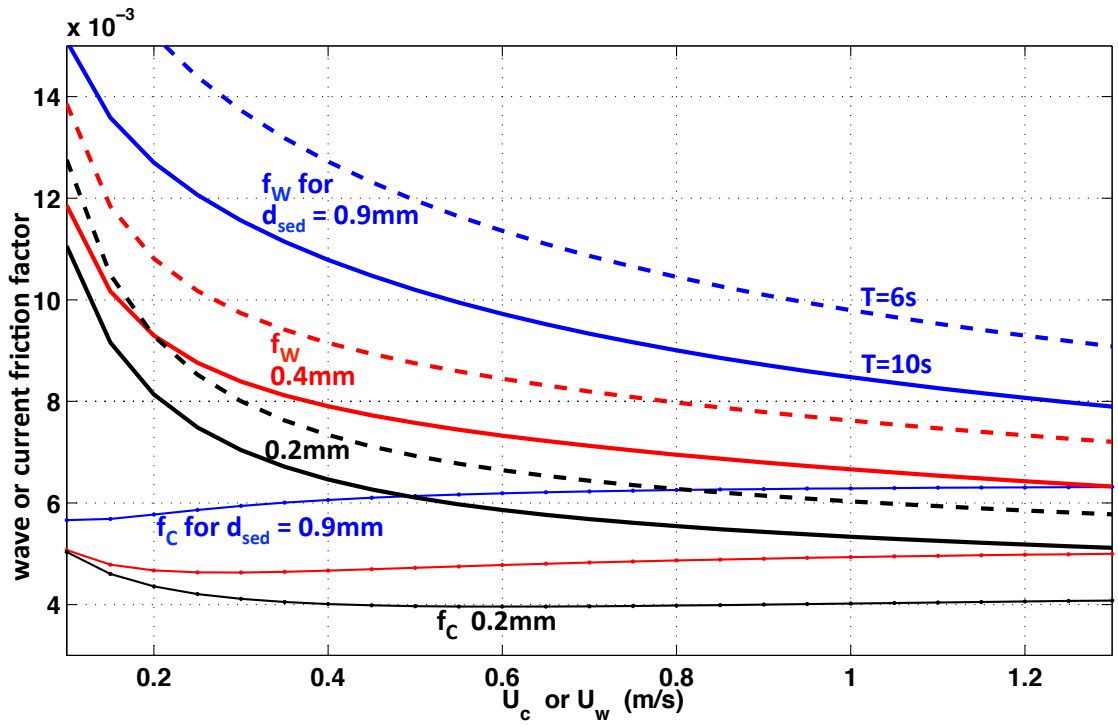

Figure 2.3. Bottom shear stress friction computed under waves (f_w) based on Myrhaug [1989] and under currents (f_c) based on Yalin [1992] for varying sediment grain sizes. For f_w, two waves periods are shown: T = 6 s (dashed) and T = 10 s (solid line).

2.4 Burial Dependence on Angle of Attack

The flow angle of attack, α, is defined as the angle between the UXO main axis and the direction of the wave orbital velocity. For most near-shore coastal locations, wave direction is constrained to a quadrant centered about shore-normal. It has been documented that scour around pipelines is less when the angle of attack is small (velocity closer to parallel) [Sumer & Fredsøe, 2002]. This effect is also observed in the laboratory for cylinders by Cataño-Lopera & Garcia, [2007]; however, because cylinders are free to rotate, they also reported the strong tendency of cylinders to turn from an initial small angle to a larger (more perpendicular) angle. For a symmetric cylinder, the most stable position is that where the long axis is perpendicular to the flow. Tapered shapes attain a stable angle of attack depending on the relative drag of their asymmetrical ends, as observed in Rennie *et al.* [2016], where, under scouring conditions in steady currents, the tapered UXO used in these tests rotated to $\alpha = 45°$. How rapidly a UXO with small initial angle α_i can rotate to its stable (larger) final position α_f that depends on the time history of the forcing, i.e. whether it experiences flow speeds sufficient to turn the UXO prior to the onset of flow sufficiently large that it will cause scour to a depth at which it is no longer free to rotate. The

conditions required to approach a threshold of motion are discussed in Section 2.5, noting that rotation can occur at lower forcing than mobility (translational motion). In practice, neither the initial or final angle of a UXO discarded on the seabed will be known: it must be estimated from some probability distribution.

Based on a compilation of laboratory data, Friedrichs *et al*. [2016] found the dependence of burial depth on flow angle of attack to be represented by

$$f(\alpha) = \exp(-c_1(\cos\alpha - c_2)), \text{ where } c_2 = \cos\alpha_{perp}\,. \tag{2.7}$$

The angle α_{perp} is the smallest angle for which the scour behavior is the same as $\alpha = 90°$ which was found to be ~ 53°. For all $\alpha > \alpha_{perp}$, $f(\alpha)$ is set equal to one. Figure 2.4a shows the laboratory data angle of attack versus measured burial, adjusted for f(KC) and $f(U_{c||}/U_m)$, as discussed in Section 2.3.1. An exponential fit gives $c_1 = 2.5$, shown as solid blue line. This factor can have a large effect, reducing predicted B/D for UXO at small angle to the flow to less than half the burial predicted for perpendicular UXO. Note there is substantial scatter in Figure 2.4a; with $r^2 = 0.44$, the fit captures less than half the measurement variability. All the empirical relationships for the burial data are determined in log-space (either power or exponential fits), reflecting the widely varying nature of the response. Therefore, in addition to the uncertainty in specifying in-situ α at remediation sites, there is large uncertainty in the equation coefficients that best represent the physical dependence. This uncertainty can be retained in the expert system by using a probabilistic form of the equations, e.g. c_1 can be drawn from a distribution based on the confidence intervals of the empirical fit. The upper and lower bounds for the 95% confidence interval for c_1 are illustrated in Figure 2.4a as dashed red lines.

Cataño-Lopera and Garcia, [2007] investigated the behavior of cylinder rotation under varying flow angles and found it to depend on multiple factors, including the density of the UXO and the timing and strength of the flow. The total amount of rotation before burial, $\Delta\alpha$, was observed to have a mean value of +20°with standard deviation σ=14°. In addition, Cataño-Lopera and Garcia, [2007] repeated experimental runs demonstrating that a cylinder exactly parallel to the flow (α=0°) is stable and remains parallel; these measurements are the data points at α_f =0 in Figure 2.4a which exhibit strong variability in burial depth. For these runs, the UXO was placed carefully on the bed at $\alpha_i = 0$ prior to the wave and current forcing. This situation, with UXO exactly parallel to the flow, is not usual in the field. For modeling site conditions in UnMES, the probability of $\alpha_i = 0$ is expected to be quite small. For sites contaminated due to jettisoned munitions, one might assume a uniform random distribution of α_i. For remediation sites that were former firing ranges, an initial distribution of UXO angle may be peaked in the direction of firing, probably close to

shore-normal. However, several factors would act to re-distribute α_i: ambient flow during deployment would slightly torque the falling UXO towards larger α while passing through the water column, while any ripples present on the seabed will be crest-perpendicular to the waves, encouraging $\alpha_i > 0$.

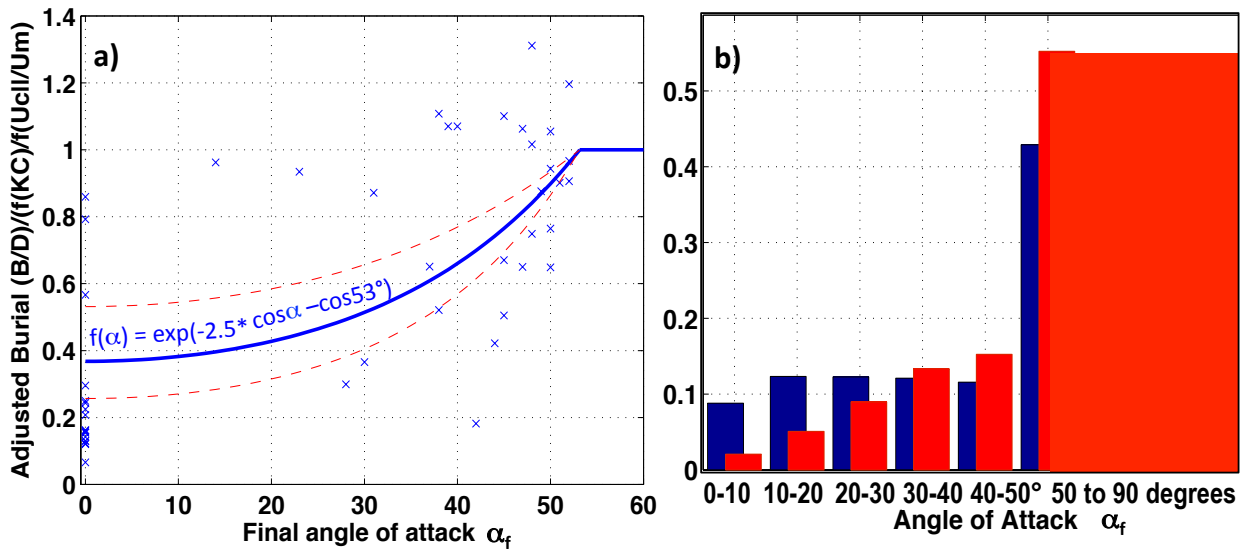

Figure 2.4. Angle-of-attack effect on UXO burial. a) multiplicative factor adjusting scour burial depth to account for dependence on angle of attack α. b) example probability distribution of α assumed to be initially approximately uniform, transformed to stable α using rotation by observed distribution $\Delta\alpha$ (Cataño-Lopera and Garcia, 2007).

For application in UnMES, a probability of α_f must be estimated based on an assumed distribution of α_i. A preliminary probabilistic relationship $\alpha_f = \alpha_i + \Delta\alpha$ is proposed where $\Delta\alpha$ is drawn from the normal distribution $P(\mu_\alpha, \sigma_\alpha)$, with $(\mu_\alpha, \sigma_\alpha)$, determined from the mean and standard deviation of the observed degree of rotation from Cataño-Lopera and Garcia [2007] as above. In Figure 2.4b, an example distribution for a field of UXO with α_i near-uniform is shown in blue. The bins selected for the UnMES α node account for the shape of $f(\alpha)$, which varies over small angles and is uniformly equal to one for $\alpha > 53°$. After rotation by $\Delta\alpha$ drawn from $P(\mu_\alpha=20°, \sigma_\alpha=14°)$, the resulting distribution for α_f is plotted in red. In this example, the majority of UXO are predicted to be effectively perpendicular to the flow, i.e, $f(\alpha) = 1$, with the average value for the UXO field is $f(\alpha) \sim 0.8$.

The available data on angle dependence exhibit unacceptably large scatter (Figure 2.4a) and supplementary research is called for. Additional laboratory observations of the effect of angle of attack have been provided by Garcia and Landry [2015], focusing on rotation

behavior on hard substrates of varying roughness. Insights gained from this data, along with more recent experiments on mobile sand beds, also performed under SERDP MR-2410, will be incorporated in to the next version of UnMES.

Table 2.1 Predictive Equations for Equilibrium Burial Fraction as implemented in Scour Burial Node, Demonstration Version of UnMES

Waves	combined shapes	$B/D = (1.85*\theta^{0.34})(\exp(-2.5(\cos(\alpha)-0.6))(0.1KC^{0.51})$	
Waves+Currents	combined shapes	$B/D = (1.85*\theta^{0.34})(\exp(-2.5(\cos(\alpha)-0.6))(\exp-1.1U_{c\|\|}/U_m)(0.1KC^{0.51})$	
Currents	cylinders (large)	clear water $\theta <= 0.04$	$B/D = 350*\theta^{2.1}$
	tapered & small cylinders		$B/D = 1200*\theta^{2.4}$
	cylinders (large)	live bed $\theta > 0.04$	$B/D = 1.2*\theta^{0.33}$
	tapered & small cylinders		$B/D = 13*\theta^{1.0}$

Table 2.1 summarizes the equations to predict equilibrium scour burial depth valid under low to moderate energy forcing ($\theta < 0.7$). High-energy burial response is expected to be dominated by density effects (Section 2.1). The application of $f(\alpha) = \exp(-2.5(\cos\alpha - 0.6))$ is included in Table 2.1 along with the dependence on KC, θ, and $U_{c||}/U_m$. Further work is needed to more gracefully determine the transition between wave- and current-dominated conditions as well as the transition from scour to fluidization as energy increases. In addition, the dependence on the angle of attack under steady currents is not yet well constrained. These topics will be pursued in future version of UnMES.

2.5 Inclusion of Inertial Factor in Mobility Threshold

In the preliminary design of UnMES, Rennie and Brandt [2015] incorporated a model for the onset of motion based on a force balance based on the analysis of Friedrichs [2014]. The relevant parameter is the mobility number, or Object Shields parameter, Θ_{obj}

$$\Theta_{\text{obj}} = \frac{U^2}{g\,(S_{obj}-1)D} \tag{2.8}$$

similar to Equation 2.1 but with the object diameter, D, replacing the characteristic sand grain size, d_{sed}, and the specific gravity of the UXO, S_{obj}, replacing the specific gravity of the sand grains S_{sed}. The stabilizing forces were found to be represented as a function of the

ratio of the UXO diameter to the scale of the bottom roughness, k. As a result, the critical threshold of motion was found to be

$$\Theta_{\mathbf{obj_crit}} = \boldsymbol{a_1}(D/k)^{\boldsymbol{b1}} \tag{2.9}$$

with the coefficients $\boldsymbol{a_1}$ and $\boldsymbol{b_1}$ determined empirically to be $\boldsymbol{a_1}$ = 1.64 and $\boldsymbol{b_1}$ = -0.71 using a fit to data compiled from the literature, enhanced by recent laboratory experiments [Rennie and Brandt, 2014, Rennie *et al.*, 2017]. Note that these coefficients are updated from the values published in the preliminary UnMES [Rennie and Brandt, 2015], now including the data from smaller D/k ratios that mimic partial burial. In another important modification from the preliminary UnMES, the near-bed U under wave-driven conditions is based on H_{10}, the largest 10% of the waves, rather than H_{sig}, since the onset of mobility can occur instantaneously. Therefore it can be forced by a single large wave, as compared to burial processes which take a time period on the order of tens of minutes to develop. Assuming the wave height probability density function (PDF) follows a Rayleigh distribution, $H_{10} = 1.27\ H_{sig}$ [Dean and Dalrymple, 1991].

In order to determine the threshold of motion under increasing currents in laboratory experiments for objects resting on sand, Rennie *et al.* [2017] estimated the flow acceleration, dU/dt, as a linear fit over the measured velocity in the laboratory test tank. The inertial effect was quantified as an adjustment factor, f_I, to the mobility force balance formed as

$$f_I = (F_D^2 + F_I^2)^{1/2}/F_D \approx 1 + (C_I/C_D)\ D\ (dU/dt)/U^2 \tag{2.10}$$

where F_I and F_D are the inertial and drag forces, respectively. The ratio of the inertial to drag coefficients was set to be $C_I/C_D \approx 2$, based on work by Sumer & Fredsøe [2002]. The effective mobility number is then calculated as $f_I\ \Theta_{obj}$. For observed current accelerations of 4 to 8 cm/s^2, the factor f_I can increase the effective mobility number by 20 to 40%.

When considering orbital velocities under waves, the acceleration effect is quantified as an inverse relation to the Keulegan-Carpenter number, KC. In this case, the adjustment factor is formed as

$$f_I = (F_D^2 + F_I^2)^{1/2}/F_D \approx (1 + 16\pi^2\ (C_I/C_D)^2\ (KC)^{-2})^{1/2}\ , \tag{2.11}$$

[Rennie *et al.*, 2017] with $C_I/C_D \approx 2$ for KC < ~30. The f_I factor was used to correct threshold of motion for mobility data under waves [Williams, 2001] before inclusion in the data compilation used to determine the best fit coefficients reported above. This factor can be very large for small KC. For most munitions in realistic conditions, KC near the threshold

of motion is large, usually KC ≥ 15, for which f_I ranges between 1 and 2. Because this factor is substantial, the Demonstration UnMES will apply f_I in the model for the migration node. The effect of including this factor will be assessed using data from field experiments in Section 3. Comparison will be made between the observed flow and the critical velocity computed as

$$U_{crit} = \mathrm{sqrt}(\Theta_{\mathbf{obj_crit}}\ g\ (S_{obj}-1)\ D\ )/\ f_I\ . \qquad (2.12)$$

2.6 Migration Distance

One of the largest gaps in our knowledge relevant to UXO burial and migration is a documented model to quantify the distance traveled after the threshold for motion is surpassed. Earlier SERDP field tests [e.g. Wilson *et al.*, 2008] using "dumb" surrogates, required diver observations to note change in UXO location. As dives were conducted weeks or even months after deployment, only cumulative migration distance could be inferred. Recent field experiments [Traykovski and Austin, 2017] have used "smart" munitions, with embedded IMU and acoustic pingers that allow determination of motion activity and location tracking in near real time.

The Migration Distance node in the Demonstration UnMES currently uses a rule-of-thumb approach guided by these field observations, similar to that in Rennie and Brandt [2015] where distance is simply assumed to be some function of $\Theta_{\mathbf{obj}}$ exceedance over $\Theta_{\mathbf{obj_crit}}$. The algorithm to construct the CPT has been adjusted to reflect the results from Traykovski and Austin, [2017] where migration distances of tens of meters were measured for mobility number $\Theta_{\mathbf{obj}}$ larger than, but still the same order of magnitude as $\Theta_{\mathbf{obj_crit}}$. The code for this provisional algorithm, found in Appendix B, removes the need for the intermediate nodes for the D/k ratio and exposure that was used in the prior (preliminary) version of UnMES. Continued research into improved quantification of migration distance will be an important future focus.

3. Prediction Performance Assessment

The ability of UnMES to make valid predictions of UXO burial and mobility will be assessed in two ways. First, the process models will be compared in a deterministic manner against available field data driven by the time-series measurements of environmental forcing. Second, the skill of the probabilistic output from the BN is quantified in comparison to baseline predictions representing "no knowledge".

3.1 Scour Burial and Mobility during TREX13

A field test in the Gulf of Mexico, the Target and Reverberation Experiment (TREX13) [Calantoni *et al.*, 2014], was undertaken in the spring of 2013, where fields of surrogate UXO with a wide variety of shapes and densities were carefully laid by divers at two sites offshore of Panama City at 7.5m and 20 m depth. At both sites quadpods mounting several instruments measured the waves, currents and sediment suspension during the month-long deployment. Each quadpod included sector scanning and pencil beam sonars to continuously monitor munitions mobility of in their field of view.

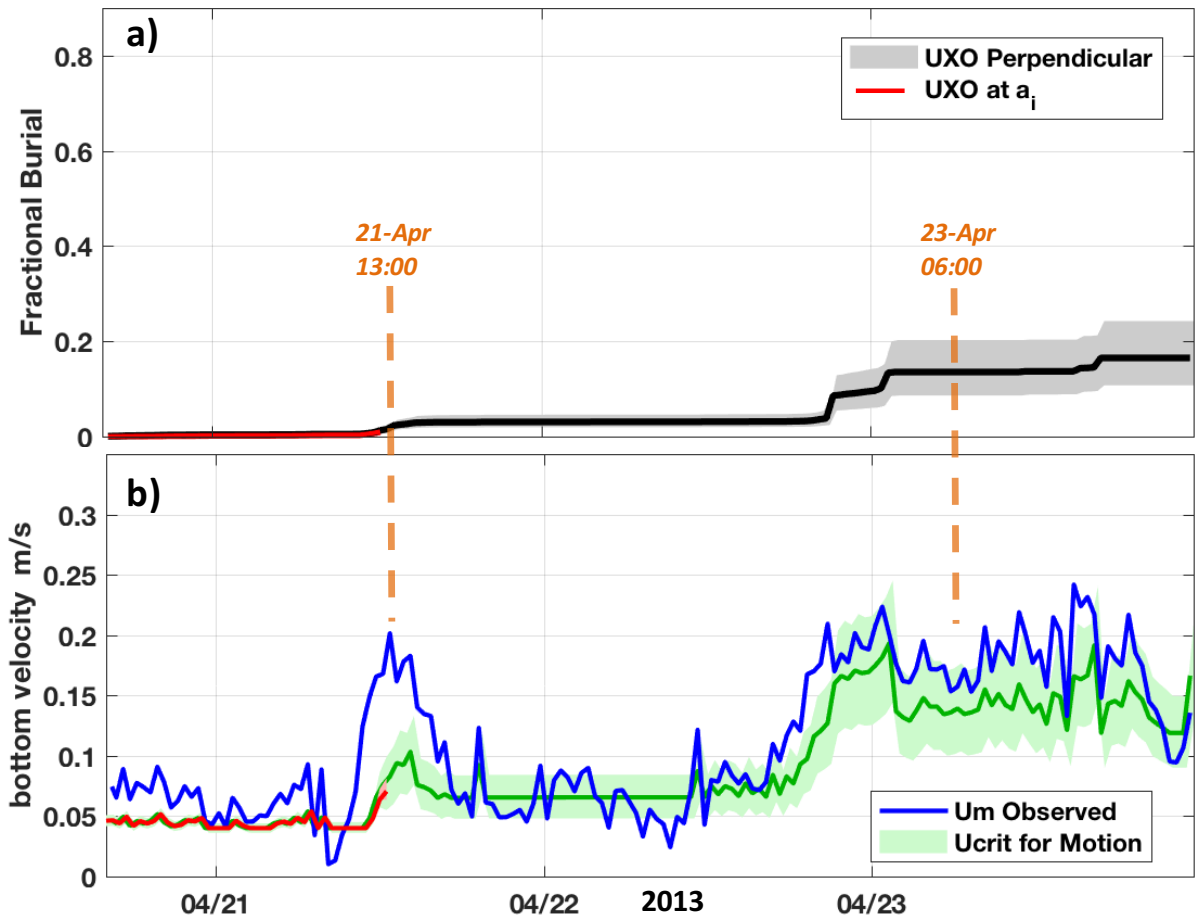

Figure 3.1 (a) Burial and (b) critical velocity for low-density UXO "C2" during early days of TREX13. Dashed lines mark times of rotation and mobility observed in sector sonar images.

Early in the deployment, the very light UXO (S_g = 1.2) were observed in the sector-scanning imagery to rotate, then to move away (beyond the field of view). The cumulative burial predicted during the first four days of the TREX13 deployment for the light "C2" UXO (shaped like a 81mm mortar) is plotted in Figure 3.1a; red line indicates burial at the initial

angle (known at the time of deployment); black line is burial for the UXO lying perpendicular to the flow. The grey shaded area indicates the confidence range for the burial prediction, combining the coefficient 95% C.I. intervals for the θ and KC fits in quadrature. The lower panel, Figure 3.1b, shows the measured near-bed flow in blue, and in green the critical flow velocity (U_{crit}) computed for onset of motion based on the predicted burial. The green shaded area again represents the 95% C.I. about the empirical coefficients in the mobility equation (Eq 2.9) combined with the burial uncertainty. The times of observed rotation (13:00 21-Apr-13) and mobility (06:00 23-Apr-13), marked as dashed lines, can be seen to occur when the near-bed flow is larger than the predicted critical velocity, indicating that the process models give reasonable results in this application.

During TREX13, after several weeks a storm occurred on May 5th and 6th with peak H_{sig} of 2 m/s recorded (Figure 3.2a). After the storm, divers visited the deep site and recorded partial burial. At the shallow site they found all but one of the UXO fully buried. In Figure 3.2 the predicted burial and corresponding critical velocity for mobility are shown in the middle and lower panels, for calculations based on the large "howitzer" UXO (diameter of 15.5 cm with S_g = 2.6). Again, burial is computed for the initial deployment angle α_i (red) and a perpendicular angle (black). U_{crit} computed for perpendicular flow is plotted in green (Figure 3.2c), and at no time does the measured near-bed flow (blue) exceed the required critical value for motion. Appropriately, no mobility was observed. However, the sonar images detected rotation of the howitzer shape occurring about 15:00 05-May-2013, which aligns with the time period when the flow is very close to the critical threshold (vertical dashed line). Following rotation, the images show the UXO perpendicular to the flow and rapid burial. The final burial prediction has a large degree of uncertainty, ranging from half to fully buried, which encompass the observations. Note that the predicted U_{crit} required for mobilization would have exceeded the proposed threshold for fluidization conditions; under these conditions a different burial regime would have ensued.

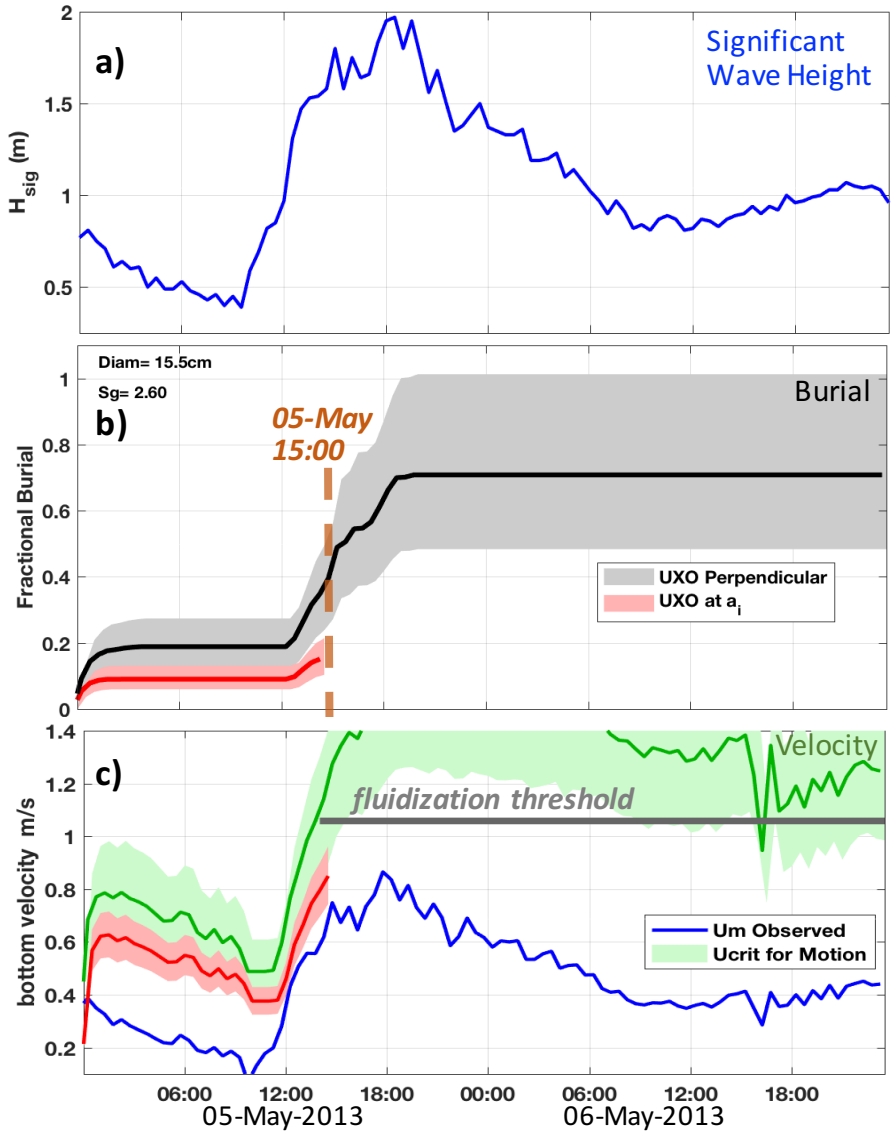

Figure 3.2 (a) Wave height, (b) scour burial and (c) critical velocity for moderate density UXO "D3" during TREX13 storm. Vertical dashed line marks time of rotation in sector sonar images.

After the storm, on 08-May the divers dug out the UXO at the shallow site and reset them as in the original plan, so that observations at that site can be treated as two deployments. Following an extended period of fairly calm conditions, divers retrieved all the remaining UXO from both sites in late May. In order to make quantitative burial estimates from TREX13 several dozens of diver photographs were analyzed visually with burial categorized into 5 burial states: less than 20% buried; 20 to 50%, 50 to 75%, 75 to 100% burial, and a state for burial deeper than the full diameter of the UXO. The burial ranges were estimated separately for 3 types of UXO, bullets (both 20 and 25mm diameters), 81 mm mortars, and a 155m howitzer shape. Note that conditions were never energetic

enough to reach the threshold for fluidization (Section 2.2); therefore, the 3 UXO shapes were grouped without regard for density.

The burial observations, along with the matching model predictions, are summarized as whisker plots on Figure 2.2 overlaid on the Friedrich *et al.,* [2016] data from which the process models were developed. The bars ($\pm\sigma$) in magenta represent conditions at the shallow site following the storm; the dark blue bars for the shallow site second deployment in quiet conditions; and the light blue represent the deep site values after the full deployment. Overall, the deterministic predictions reasonably agree with the observations (r^2 = 0.86). Partial burial tends to be overestimated, while complete, full burial can be underestimated.

3.2 Mobility at Long Point, Martha's Vineyard

A field experiment conducted in September 2014 at Long Point Wildlife Refuge on Martha's Vineyard by researchers at WHOI [Traykovski and Austin, 2017] was located closer to the beach than TREX13, in depths between 2 to 4m, and measured more energetic conditions. The time-series of hydrodynamic forcing was compiled from measurements taken at the Martha's Vineyard Coastal Observatory (MVCO) offshore in 12m depth, an instrumented quadpod deployed at 4.5 m depth, and a pole-mounted Acoustic Doppler Velocimeter (ADV) closer to shore. The bottom orbital velocity of the shoaling waves was transformed from the measurement site to the UXO location using estimates based on the SWASH model as described in Traykovski and Austin [2017]. Predictions for two groups of surrogate UXO are plotted in Figure 3.3: group "D" deployed on 16-Sep in depth between 3.4 to 4.2 m; and group "S" deployed on 19-Sep in shallower depths (between 1.8 to 3.4 m) further inshore. All these UXO had a diameter of 14 cm, but their density varied from S_g = 1.8 to 3.7. The time at initiation of motion (plotted as open circles) is determined from the IMU embedded in each UXO.

The predicted burial for the "D" deployment is shown Figure 3.3a, again exhibiting a wide range of uncertainty (grey shaded region). The maximum θ computed for these conditions is less than 0.7, hence no sheet flow is predicted, and therefore no density-dependent burial. The initial angle of the deployment is unknown, so an angle is assigned representative of the average α_f discussed in Section 2.4.

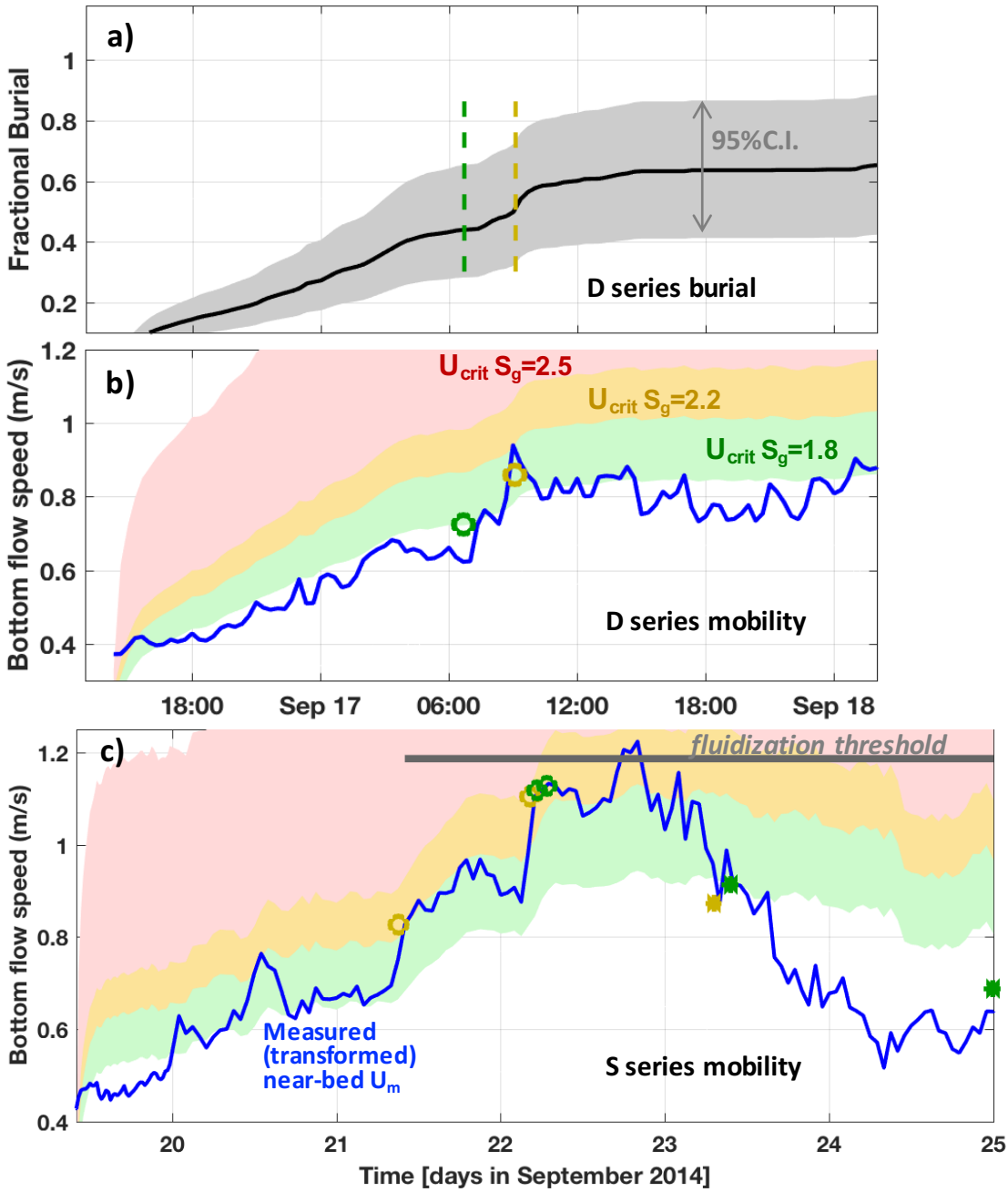

Figure 3.3 (a) Burial and (b) critical velocities for group 1 "D series" UXO of three densities predicted for Long Point surf zone field experiment and (c) critical velocities for group 2 "S series".

Because the threshold of motion is very sensitive to fractional burial, this causes a broad area of uncertainty in the required critical velocity, plotted in Figure 3.3b as regions shaded with colors representing the different UXO densities: green for "light" (S_g = 1.8), gold for "medium" (S_g = 2.2), and pink for "heavy" (S_g = 2.5). The transformed flow measured near-bed (blue) is less than all the critical thresholds, except for a short period during 17-Sep at

about 07:00. Marked on Figure 3.3a as vertical dashed lines are the observed times of motion initiation; these and the circles on the velocity plot, are plotted with color indicating density. The mobility events are observed occur during the period when the measured velocity is closest to the predicted critical value.

The bottom panel of Figure 3.3 shows the critical velocity regions computed for three UXO densities during the time period following the "S" deployment farther inshore. In this application, the measured flow exceeds the lowermost threshold for S_g = 1.8 (green) for much of the time, and reaches the threshold predicted for S_g = 2.2 (gold) at several locations. The UXO with those densities were observed to migrate (open circles), while it was observed that none of the "heavy" UXO became mobile, consistent with the predictions where the measured flow (blue line) does not reach the pink shaded region indicating motion for "heavy" S_g = 2.5. After midday 21 September, the predicted flow speed required to mobilize the heavy UXO would have entered the fluidization regime, so that the burial would have become density dependent (Section 2.2). The solid symbols marked times when motion of UXO with S_g=1.8 and S_g=2.2 stopped; these times correspond reasonably with when the flow drops lower than the computed motion thresholds.

Application to the Long Point surf zone data shows that our current process models are generally reasonable. However, dependence on accurate burial prediction compounds the uncertainty: if partial burial is over-predicted, no mobility is expected. Analysis of the Long Point data by Traykovski and Austin [2017] concluded that it is crucial to correctly predict the time-dependent evolution of burial, and that the timescale for burial must be substantially longer than that reported in previous work, e.g. Demir and Garcia [2007], discussed in Rennie *et al*. [2017]. Traykovski suggests a timescale about 5 times longer; a number of timescale factors were explored for the predictions presented here and small differences were observed. Given a timescale dependence, the rate at which environmental forcing increases, i.e. the arrival speed of a storm, is an important factor. Further research into the role that timescale of burial plays will be undertaken in MR-2645.

3.3 Probabilistic Performance

The CPT for each child node in the Bayesian Network (BN) forming the burial and migration core of UnMES (Figure 1.1) is populated by sampling numerous combinations of the input variables using a Monte Carlo (MC) approach and applying the equations documented in Rennie *et al.* [2017], Friedrichs *et al.* [2016], and in Section 2 above. The MC simulation is implemented in MATLAB and samples from probability distributions appropriate to each input variable: wave height is drawn from a lognormal PDF; wave

period from a normal PDF, and the other inputs from uniform distributions. The parameters describing the input node PDFs can be specific to the geographic region being modeled. Each continuous variable, or node, in the BN is discretized into some number of states or bins; the width of each bin chosen appropriate to how well that parameter can be resolved [Rennie and Brandt, 2015]. Some nodes are naturally discrete, e.g. UXO type.

The Demonstration BN is designed to be auto-generated at each cell located within a spatial structure (Section 4), therefore the values for water depth & sediment are fixed, eliminating those nodes from the sampling requirements. For the CPT of the node representing burial due to scour and fluidization, there are six "parent" nodes, which have between 3 to 10 states, resulting in a multi-dimensional probability table with over 30,000 entries. A Monte Carlo set of over 1 million simulations is incorporated as a case file by Netica to train the BN. With the network structure specified, and the data fully observed by extensive MC simulation, it is appropriate to use Maximum Likelihood learning for the conditional probability table values, examples of which are shown in Appendix C. The observed environmental forcing is entered at the input nodes (marked blue in Figure 1.1). The distribution of UXO types and angles (if known) are additional input nodes. As illustrated in Figure 3.4, twice as many bullet-like UXO were deployed in TREX13 as the larger surrogates, so the representative input distribution is specified as half "bullet" types, a quarter "mortar" and a quarter "howitzer" types.

The ultimate goal for UnMES is to model UXO behavior over extended time periods, representative of years or even decades corresponding to time periods for which the contaminant munitions may have been present at the site. The available field data represents short periods (weeks), which here will be partitioned and treated on "event" time scales of hours to days in order to evaluate our current process models' predictive capability for burial and onset of mobility. Each event is represented by its peak forcing: the largest wave heights observed, along with the concomitant wave period and observed currents. Future work will examine the best method to model an accumulation of events occurring repeatedly over a long time horizon.

For the Bayesian network UnMES, the model-data comparison is performed by comparing PDFs. There are many metrics that can be used for evaluation of the skill of a probabilistic prediction. One that is popular in the weather forecasting community is the Ranked Probability Score, a form of the Brier score [Plant and Holland, 2011]. This is most readily interpreted when normalized as the Ranked Probability Skill Score (RPSS) which is relative to some specified baseline, or reference, distribution that might be assumed if no forecast was available (i.e. a state of "no knowledge"). In weather forecasting, this baseline

distribution is usually either climatology or persistence. For our purposes, the baseline might be uniform probability – i.e. if you do not know anything about the site's munitions or its environment you might assume that all categories of burial are equally likely. Alternately, a "no knowledge" situation might be represented by a distribution with 100% in the 'fully buried" state, i.e. assume that all the UXO are totally buried. The RPSS indicates the percentage improvement that the UnMES prediction provides over a baseline assumption. RPSS is computed as the mean-square error of a multi-state forecast where observations are 1 for the observed state and 0 for all other states, normalized by the mean-square error of the reference forecast. RPSS = 0 indicates no improvement over the reference; a perfect score is RPSS = 1.

The UnMES prediction in Figure 3.4a represents equilibrium burial during the calm period (2nd deployment 08-22 May 2013) at the TREX13 shallow site. This BN was generated with the water depth fixed at 7.5 m and the sediment specified as fine grain sand. Following two quiet weeks (maximum observed wave height less than 1 m), the burial distribution predicted has the mode in the 2nd state representing 20-50% burial, with also some burial predicted in the surrounding states. The histograms of observed burial from TREX13 (shown in blue in Figure 3.4b) are based on sample numbers ranging from ½ dozen to 2 dozen analyzed photographs. The observations at the shallow site Figure 3.4b had a distribution with the mode again in the 2nd bin, but no burial in the 3 deeper states. This slight overprediction for partial burial is similar to what was reported in the deterministic summary (Section 3.1).

The lower plot in Figure 3.4b illustrates the "no knowledge" distributions; uniform burial in shown in red and total burial in green. The UnMES RPSS = 0.92 compared to the uniform assumption, and RPSS = 0.96 compared to total burial, showing that in this case UnMES predictions provide substantial improvement over the baseline burial distributions. Additional model-data comparisons for equilibrium burial from the storm period during TREX13 will be shown in Section 4. A probabilistic evaluation of mobility from TREX13 was not performed because there are not enough observations to form a distribution.

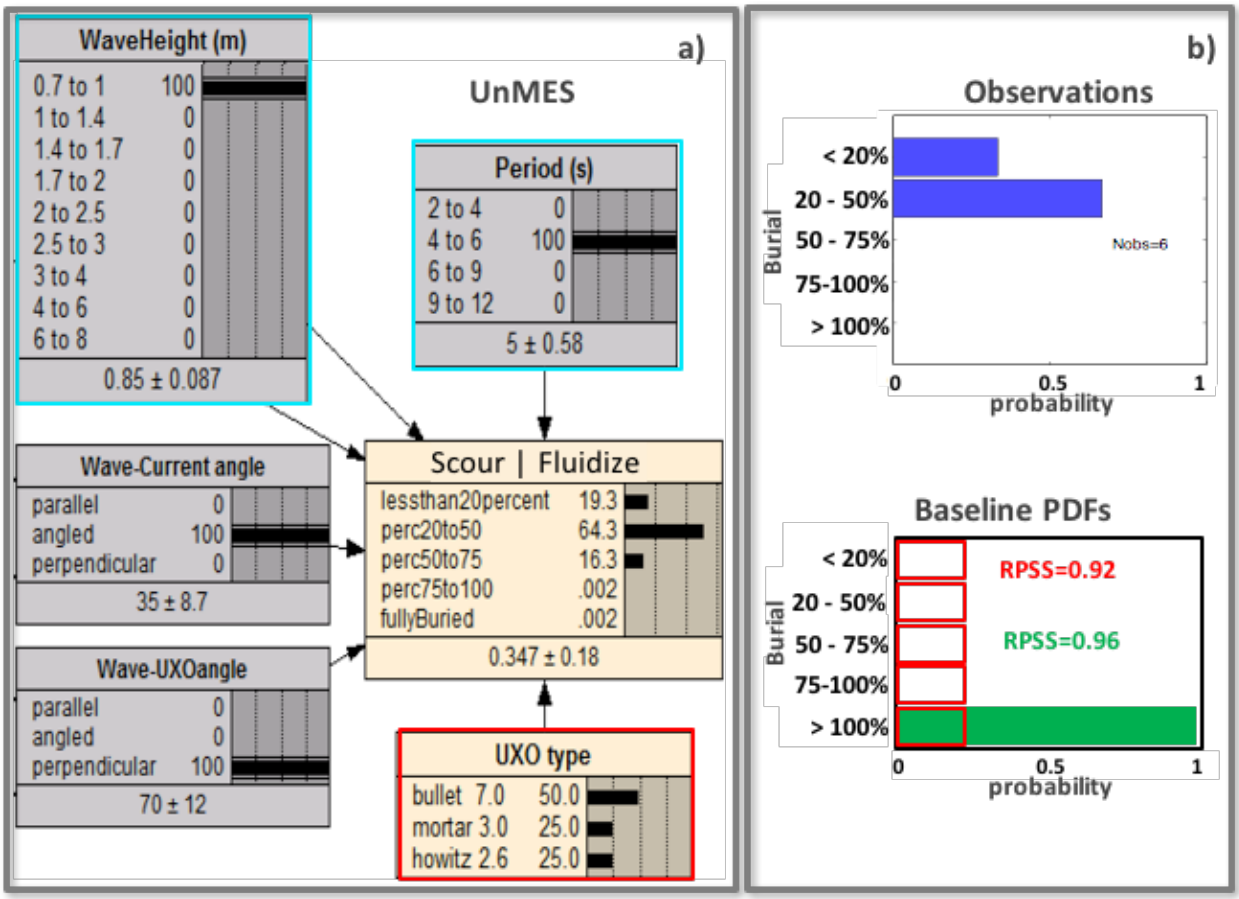

Figure 3.4 a) Probabilistic burial prediction from UnMES for conditions at the shallow TREX13 site from May 8 to 22, 2013. b) upper plot represents histogram of corresponding burial observations; lower plot is diagram of two baseline distribution (uniform and 100% burial) used to compute skill scores.

A comparison of the migration distance observed versus predicted is illustrated for the surrogate UXO deployed during the Long Point surf zone field test in Figure 3.5. As discussed in Section 3.2, UXO with several different densities were deployed: S_g = 1.8, 2.2 2.5 and 3.8 [Traykovski and Austin, 2017]. The measured migration data, a total of 21 observations, are grouped by UXO density, and binned into distance states to form histograms (Figure 3.5a) that are comparable to the prediction PDFs from UnMES. In this implementation, the states are labeled "Stay" for UXO that do not move any significant distance; "Near" for those that move some appreciable amount, and "Far" for those migrating a distance large enough that they move into a significantly different management region or become subject to different hydrodynamic forces. The boundaries for the state intervals in the Demonstration expert system are 0 to 5 m for "Stay", 5 to 50 m for "Near"

and greater than 50 m for "Far". The boundaries for an operational UnMES implementation would depend on the management concerns and spatial scales of the actual site of interest.

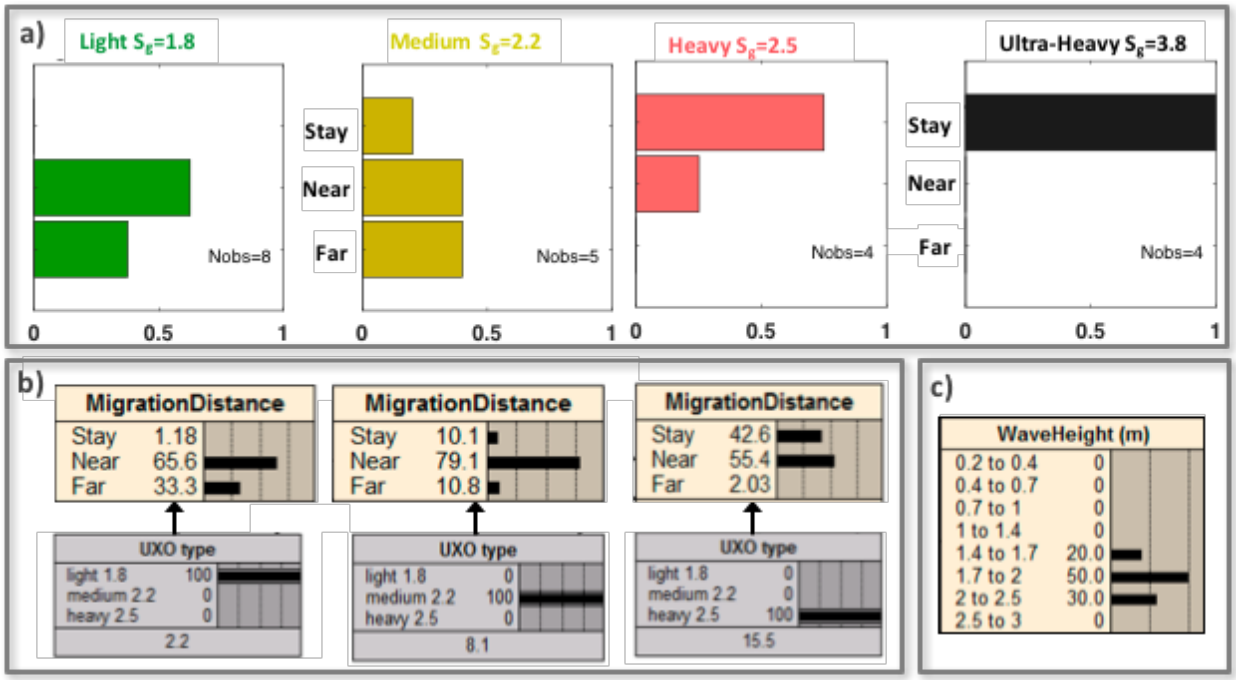

Figure 3.5 a) Histograms of UXO migration distance, grouped by density, from Long Point observations [Traykovski and Austin,2017] with state interval divisions at 5 and 50 m. b) UnMES predictions for three UXO densities, forced by waves with height distribution as in c).

Examining the observation histograms, it is obvious that UXO density is an important controlling factor in migration, as expressed mathematically in Equation 2.8. All the of lightest group migrated, and all of the heaviest UXO stayed put. The light UXO (shown in green) have densities representative of pyrotechnic munitions such as signal flares, while the heaviest are more representative of weapons. A Demonstration UnMES BN based on the water depth and sediment characteristics of the Long Point site was generated for UXO types used by Traykovski and Austin [2017]. Migration distances are estimated as an *ad hoc* function of mobility number exceedance over threshold as described in Section 2.6 (see Appendix B). The output probabilistic predictions are shown in Figure 3.5b for the "light", "medium" and "heavy" Long Point UXO, where the state intervals are the same as for the observation histograms. Values were entered in the Wave Height node (Figure 3.5c) which approximately reproduce the distribution of peak bottom velocities observed during the migrations. The state of the Scour | Fluidize burial node is set to 20-50 percent, representative of the fractional burial predicted at time of mobilization (Section 3.2).

The pattern of migration dependency on UXO density is reasonably captured by the UnMES predictions in Figure 3.5b. The light UXO are predicted to migrate 2/3 "Near" and 1/3 "Far", very similar to the observations. The medium density UXO are predicted to have the widest range, with some migration into all 3 states, as observed. Migration for the heavy UXO are somewhat over-predicted, while the heaviest (Sg = 3.8) are correctly predicted to be almost completely stationary with > 92% in "Stay" (not shown in Figure 3.5, see Appendix C). Note that because the migration distance function (Appendix B) was developed using these Long Point observations, this model-data comparison is not a validation, but merely verifies that the UnMES implementation is correct. This rule of thumb estimation functions largely as an example of how a BN migration distance node could be developed, and is a place holder for future implementation. Full validation awaits additional laboratory and field data with improved physical understanding for a more robust migration distance model.

4. Spatial Domain Provincing

Integration of the UnMES BN within a Geographic Information System (GIS) framework is proposed to resolve and display spatial variation across specific sites of interest. An example spatial implementation is illustrated using output such as would be available from a modeling effort at NRL-Stennis where nested grids of the Simulating WAves Nearshore (SWAN) model were run as part of a project to test the Navy Seafloor Evolution Archetype (NSEA), an operational spectral ripple model [Penko *et al*., 2017]. The inner grid, centered in the TREX13 location, resolved the bathymetry and waves with 444 m grid size as shown in Figure 4.1. The sediment characteristics used at each location are based on the NAVOCEANO Bottom Sediment Type database [NAVOCEANO, 2003].

The sediments mapped in Figure 4.1b show that fine sand covers all the region in between the TREX13 deep and shallow quadpod sites in water depths from 5 to 20 m, except for an area to the east of the deep site where a gravel-shell mixture is indicated. A narrow region just offshore of the beach, where cuspate sandbars can be seen, is characterized as medium sand. An UnMES Bayesian network was generated at each of the five grid cells marked with white boxes in Figure 4.1a, two of which contain the deployment sites for TREX13 where burial observations are available.

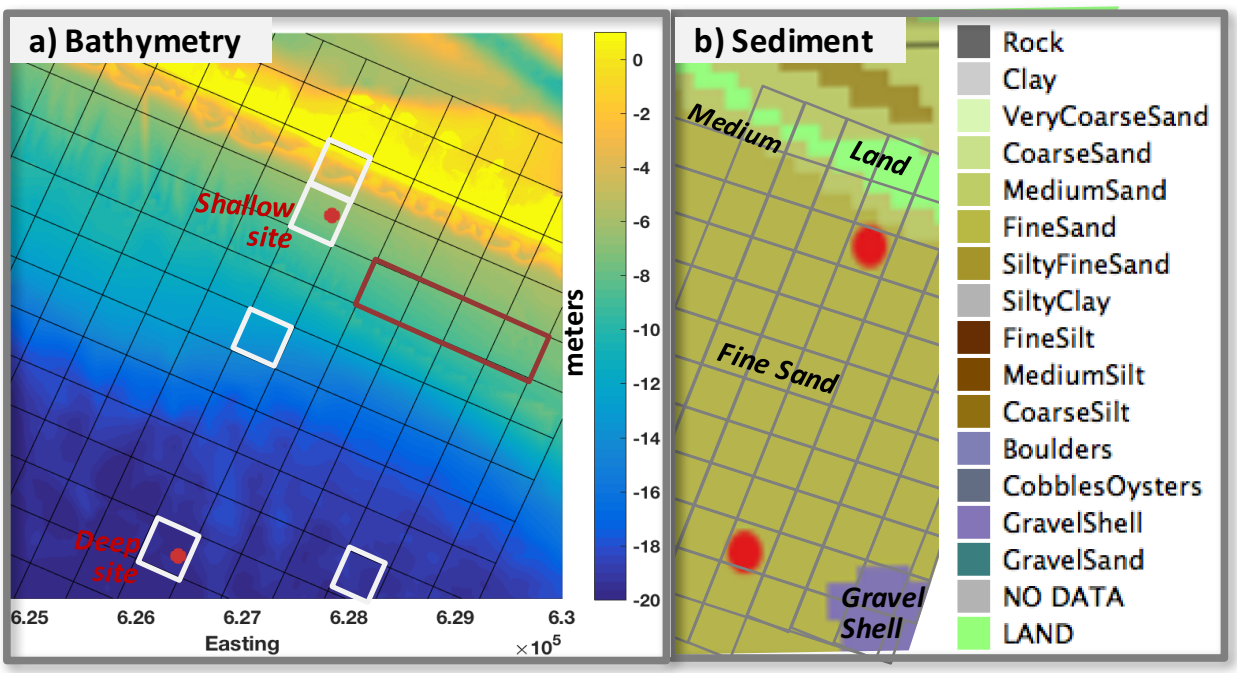

Figure 4.1 a) Bathymetry surrounding TREX13 field test location and grid representing innermost SWAN grid (444 m resolution). b) NAVOCEANO bottom sediment types (reduced categories). Red dots mark locations of TREX13 measurements.

UnMES predictions are reported in Figure 4.2 for the peak forcing experienced during the storm event of 05-06 May 2013. Instead of using in-situ measurements as from TREX13, SWAN model ouput of wave heights from nearest grid cells would be used to specify the input forcing to UnMES to illustrate the manner in which the expert system might be used in an operational setting. The wave heights for all the offshore locations lie in the same state (1.7 to 2 m), with a reduction in H_{sig} modeled for the sandbar cell (with depth of 3 m) where the state 1.4 to 1.7m is set. From top to bottom in Figure 4.2, the burial prediction PDFs show the expected decrease in scour burial as the water depth increases, reducing the wave energy felt at the bottom. At the 8 m and 20 m grid cells, the UnMES predictions can be compared to histograms of observations from TREX13. As in Figure 3.4, a distribution of 50% bullets, 25% mortars and 25% howitzers is used to most closely represent the mix of UXO in the TREX13 observations.

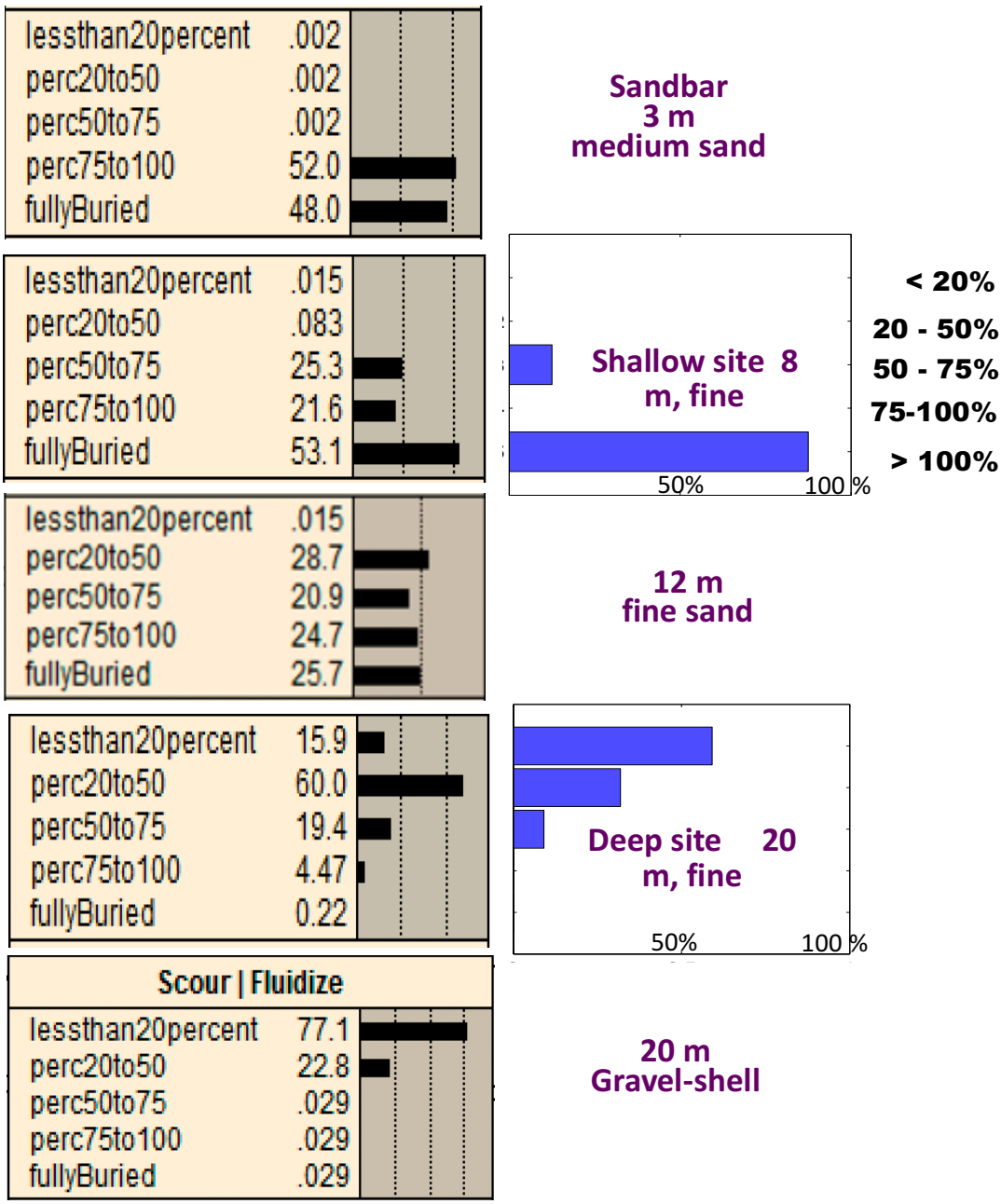

Figure 4.2 Probabilistic burial predictions at 5 cells (locations marked in Figure 4.1) from the spatially-varying implementation of UnMES. Hydrodynamic forcing from peak of 05-06 May 2013 storm as modeled by SWAN. From top to bottom, water depth is 3, 8, 12, 20 and 20 m with corresponding sediment grain sizes of 0.4, 0.25, 0.25, 0.25, and 3 mm. Observation histograms (blue) at 8 and 20 m fine sand sites compiled from diver photographs as described in Section 3.1.

UnMES slightly over-predicts burial at the deep site (RPSS = 0.65 compared to uniform assumption), but gets the mode correct at the shallow site (RPSS = 0.89). Almost complete

burial is predicted for the sandbar cell, and a wide range of burial responses are output at the intermediate 12 m cell. The bottommost PDF represents the BN generated for a water depth of 20m with gravel-shell sediment where over ¾ of the UXO is modeled is being less than 20% buried, and 23% exhibiting partial burial largely the result of bullet-size UXO.

As discussed in Rennie and Brandt [2015], gridded model cells can be provinced together to form regions where the static variables, in this case water depth and sediment grain size, fall into single states, thereby reducing the number of nets that are required. This is illustrated in Figure 4.1 where four cells are grouped together by a purple box -- the cell depths are all within a bin from 9 to 10 m and all are designated as fine sand. Therefore the same BN can be used across that 4-cell province.

5 Summary and Implications

This report discusses the progress made in the development of UnMES during the Project MR-2227 contract period (2013-2016). Models for the dependence of scour burial on shear stress, and for the onset of motion in steady flow, were introduced in the UnMES Preliminary Design Report [Rennie and Brandt, 2015]. Further work implemented in the Demonstration Version of UnMES is discussed here, including:

- The role of UXO density on burial and migration
- The effects of oscillatory flow - burial under waves
- The effects of the angle between bottom flow and the UXO
- Acceleration effects on initiation of motion
    - Incorporation of an inertial factor for mobility threshold
- Rule-of-thumb estimation of UXO burial by fluidization
- Rule-of-thumb estimation of UXO migration distance

UnMES prediction performance was assessed, specifically in terms of:

- Scour burial and mobility during TREX13 in the Gulf of Mexico
- Mobility at Long Point, Martha's Vineyard experiment
- Overall probabilistic performance

The overall deterministic prediction performance for UXO burial assessed with time series driven by in-situ measurements of the environmental forcing is acceptable, accounting for

over 80% of the observed variability; however there is a wide range of scatter. Predictions judged in a probabilistic construct indicate that the Demonstration Version of UnMES produces forecasts that provide improved guidance over uninformed baseline distributions. In addition, an example of spatial domain provincing is presented. This approach will lead to a viable utilization of UnMES for site remediation support and risk analysis investigations.

Achievement of the ultimate goal of having a computer based tool for prediction of mobility and burial of underwater munitions to guide remediation management can be achieved through the directed input to UnMES from associated SERDP MR studies that will provide: updated process models; regional numerical models for predicting fluid and sediment transport at remediation sites; and field data for use in model development and validation. Although the phenomenology of different mechanisms may be investigated independently to improve our understanding, in reality they interact on numerous scales. The expert system provides an integrated prediction whereby the interdependence of multiple phenomena is made explicit.

Based on the analysis to date as described in the present report, in order to provide a comprehensive probabilistic expert system for UXO burial and migration prediction, a number of areas requiring further investigation and modeling have been identified. These topics will be investigated in SERDP project MR2645 ("Underwater Munitions Expert System for Remediation Guidance," 2016-2019) in conjunction with the related projects supported by the SERDP MR program.

Specific areas requiring further investigation can be grouped into two categories.
Phenomena that occur locally over short time scales include:

- Impact burial of munitions entering the water at high speeds
- Effect of angle-of-attack on subsequent burial in mobile sand beds
- Specification of the transition between wave- and current-dominated conditions
- Specification of the transition from scour to fluidization as energy increases
- The role of granular sorting phenomena in UXO burial
- The role of time-varying pressure-gradient forces in causing fluidization
- Improved quantification of migration distance after onset of mobility
- The role of timescales of environmental forcing, e.g. the arrival speed of storms, on UXO burial and mobility onset

Incorporating farfield processes that transpire over moderate to long time scales will require research into:

- Modeling the effects of the migration of bedforms, such as ripples and sand waves, on UXO burial and mobility
- Aggregation of repeated mobility instances
- Improved prediction of infrequently-occurring extreme events
- Methodology appropriate for modeling accumulation of extreme events occurring over a long time horizon

In addition, optimal development of subsequent versions of UnMES will need to understand what are the primary user issues. For this, input from the remediation community at large is required. Key general issues include:

- Site specific information on munition types and specifications of their initial deployment
- Information of the past and current environmental conditions, e.g. sediment types, depth changes, at the site of interest
- The level of temporal and spatial detail that would most beneficially support remediation efforts and risk assessments

Problems of short time and space scale phenomena can be effectively solved by focused research into each process individually using an approach that includes field experiments, supplemented by laboratory studies that are specifically designed to observe transitions into high-energy forcing conditions. Understanding of long time scale behavior will require translating results obtained from coastal geomorphology research to infer munitions behavior in the context of evolving seabed configurations. The most relevant information may come from remediation sites that have a long monitoring history. Funded partnerships between SERDP researchers and managers at relevant sites would be of significant benefit. These partnerships would also provide the required user input into design of UnMES products to effectively convey probabilistic expert system output in a manner accordant with user requirements.

Appendices

Appendix A: MATLAB code for predicting Scour burial and onset of mobility.

Appendix B: Rule of Thumb algorithms estimating fluidization and migration distance

Appendix C: Example CPT

Appendix D: Scientific and Technical Publications from MR-2227

Literature Cited

Calantoni, J., T. Staples and A. Sheremet, 2014. "Long Time Series Measurements of Munitions Mobility in the Wave-Current Boundary Layer," SERDP Project MR-2320, Draft Interim Report.

Calantoni, J., 2016. "Long Time Series Measurements of Munitions Mobility in the Wave-Current Boundary Layer," SERDP Project MR-2320, In-Progress Review.

Cataño-Lopera, Y.A., M.H. García, 2006. Burial of short cylinders induced by scour under combined waves and currents. *ASCE Journal of Waterway Port Coastal and Ocean Engineering* 132(6): 439-449.

Cataño-Lopera, Y.A., M.H. García, 2007. Geometry of scour hole around, and the influence of the angle of attack on the burial of finite cylinders under combined flows. *Ocean Engineering* 34, 856-869.

Cataño-Lopera, Y.A., S.T. Demir, & M.H. García, 2007. Self-burial of short cylinders under oscillatory flows and combined waves plus currents. *IEEE Journal of Oceanic Engineering* 32(1): 191-203.

Clement, C. P., H. A. Pacheco-Martinez, M. R. Swift, P. J. King, 2010. "The water-enhanced Brazil nut effect", EPL *Europhysics Letters*, Vol. 91 54001.

Dean, R. G., R. A. Dalrymple, 1991. Water wave mechanics for engineers and scientists. Vol. 2. World Scientific Publishing Co Inc.

Demir, S.T., M.H. García, 2007. Experimental Studies on Burial of Finite Length cylinders under Oscillatory Flow, *J. Waterway, Port, Coast, and Ocean Eng., ASCE, 133* (2), 117-124.

Fahnestock, R. K., W. L. Haushild, 1962. Flume Studies of the Transport of Pebbles and Cobbles on a Sand Bed, Geological Society of America Bulletin, v. 73, p. 1431-1436.

Friedrichs, C.T., 2014. "Simple parameterized models for predicting mobility, burial, and re-exposure of underwater munitions: SERDP MR-2224." Strategic Environmental Research and Development Program, In-Progress Review Meeting for the Munitions Response Program Area, Arlington, VA, http://www.vims.edu/chsd, May 21, 2014.

Friedrichs, C.T., 2016. "Parameterized Process Models for Underwater Munitions Expert System", Proposal for SERDP project MR-2647.

Friedrichs, C.T., S.E. Rennie, A.Brandt, 2016. "Self-burial of objects on sandy beds by scour: A synthesis of observations," J.M. Harris, R.J.S. Whitehouse, S. Moxon (eds.), Scour and Erosion. CRC Press. 179-189.

Foster, D.L., A.J. Bowen, R.A. Holman, P. Natoo, 2006. "Field Evidence of Pressure Gradient Induced Incipient Motion", *Journal of Geophysical Research*, 111(C5), C05004, 1-8.

Garcia, M., 2008. "Sediment Transport and Morphodynamics", In: *Sedimentation Engineering: Processes, Measurements, Modeling, and Practice*, 21-163, M. Garcia, Ed., ASCE.

Garcia, M., B. Landry, 2015. "Large-Scale Laboratory Experiments of Incipient Motion, Transport, and Fate of Underwater Munitions under Waves, Currents, and Combined-Flows", Interim Report, SERDP Project MR-2410.

Jenkins, S., G. D'Spain, J. Wasyl, 2013. "Hydrodynamic Mobility Analysis of UXO Transport, Andrew Bay Adak Island, Alaska," Scripps MPL Report to Munitions Response, Battelle, 99 pp.

MATLAB version R2014B 2016. The MathWorks Inc., Natick, Massachusetts.

NAVOCEANO, 2003. "DATABASE DESCRIPTION FOR BOTTOM SEDIMENT TYPE (U)", OAML-DBD-86, Naval Oceanographic Office, Acoustics Division, Stennis Space Center.

Norsys, 1995–2017. Netica™ of Norsys Software Corp., Ver. 5.15, www.norsys.com.

OSPAR,2013."Encounters with Chemical and Conventional Munitions," http://www.ospar.org

Penko, A., J. Calatoni, B. T. Hefner, 2017. "Modeling and Observations of Sand Ripple Formation and Evolution During TREX13", IEEE Journal of Oceanic Engineering, 42, No. 2. pp 260-267.

Plant, N. G., K.T. Holland 2011. Prediction and assimilation of surf-zone processes using a Bayesian network. Part II: Inverse models, *Coastal Eng., 58* (1), 256-266.

Rosato, A, K. J. Strandberg, F. Prinz, R.H. Swendsen, 1987. "Why the Brazil Nuts Are on Top: Size Segregation of Particulate Matter by Shaking", Phys. Rev. Lett. Vol.58, 1038–1040 (1987).

Rennie, S.E., A. Brandt, 2014. "Experimental Determination of Underwater Munitions Mobility and Burial," Johns Hopkins Univ. Applied Physics Laboratory Technical Memorandum FPS-T-14-0575, December 2014.

Rennie, S.E., A. Brandt, 2015. "Underwater Munitions Expert System: Preliminary Design Report," Johns Hopkins Univ. Applied Physics Laboratory Technical Memorandum FPS-T-15-0333, August 2015.

Rennie, S.E., A. Brandt, C.T. Friedrichs, 2017. "Initiation of motion and scour burial of objects underwater," *Ocean Engineering*, Vol 131, 282-294.

Sarpkaya, T., 1986. "Force on a circular cylinder in viscous oscillatory flow at low Keulegan-Carpenter numbers" J. Fluid Mech, Vol. 165, 61-71.

Soulsby, R. 1997 Dynamics of Marine Sands, HR Wallingford, Thomas Telford, London.

Sumer, B. M, A. Kozakiewicz, J. Fredsøe , R. Deigaard 1996. "Velocity And Concentration Profiles In Sheet-Flow Layer Of Movable Bed", Journal of Hydraulic Engineering, 122(10): 549-558.

Sumer, B. M, J. Fredsøe 1990. "Scour below Pipelines in Waves", Journal of Waterway, Port, Coastal and Ocean Engineering, Vol. 116, No. 3, 307-323.

Sumer, B.M, J. Fredsøe, 2002. *The mechanics of scour in the marine environment*, World Scientific, Singapore.

Sumer, B.M. 2014. *Liquefaction around marine structures*. Singapore: World Scientific.

Traykovski, P., T. Austin, 2017. "Continuous Monitoring of Mobility, Burial, and Re-Exposure of Underwater Munitions in Energetic Near-Shore Environments," SERDP Project MR-2319, Final Report, 44pp.

Viparelli, E., L. Soralli, K. M. Hill, 2015. “Downstream lightening and upward heavying: Experiments with sediments differing in density”, Sedimentology, Vol 62, 1384-1407.

Voropayev, S.I., G.B. McEachern, D.L. Boyer, H.J.S. Fernando, 1999. Dynamics of sand ripples and burial/scouring of cobbles in oscillatory flow. *Applied Ocean Research* 21(5): 249-261.

Voropayev, S.I., F.Y. Testik, H.J.S. Fernando, D.L. Boyer, 2003. Burial and scour around short cylinder under progressive shoaling waves. *Ocean Engineering* 30(13): 1647-1667.

Whitehouse, R. 1998. Scour at Marine Structures, HR Wallingford, Thomas Telford, London.

Wilson, J. V., I. McKissick, S.A. Jenkins, J. Wasyl, A. DeVisser, B. Sugiyama, 2008. “Predicting the Mobility and Burial of Underwater Munitions and Explosives of Concern Using the VORTEX Model,” Final Report, ESTCP Project MM-0417.

This page is blank

Appendix A: Matlab code for predicting burial and onset of mobility.

Code to perform Monte Carlo simulations:

1) mc_scour_DemoVersion.m
   script which calls equilib_scourmc_fluidize_DemoVersion.m
   which calls fluidize_estimate_DemoVersion.m (see Appendix B)

2) mc_migrate_DemoVersion.m
   script which calls mobility_migrate_DemoVersion.m
   which calls migrate_estimate_DemoVersion.m (see Appendix B)

*** mc_scour_DemoVersion **********

```
%  mc_scour_DemoVersion   April-June 2019   Script for Monte Carlo exploration of
scour and fluidization model for UnMES.
%  Version where a UnMES Bayesian Network (BN)is built for each fixed spatial province (may be
%  a single grid cell) therefore  WaterDepth and Sediment Grain Size are
%  specified as scalar values.
%  UXO type is a structure, with separate output file written for each UXO type
%  for pratical purposes to constrain output file size. Written out in Ascii columns
%   which is directly readable with Netica's Learn > Incorporate Case File
%    S. E. Rennie    JHU/APL   June 2017

UXO.type = 'bullet';  % Single UXO type set  for each run of this script
UXO.Sg   = 7.0;       % specific gravity  e.g.  Sg = 7.0 for Bullet,  Sg = 3.0 for Mortar
UXO.Diam = 0.025;     % meters    e.g. D = 25mm for bullet, 81mm for Mortar and 155mm for Howitzer

Waterdepth = 12;   % fixed for each run of this script
dsed       = 0.25 ;  % mm   0.25 fine sand     0.4m medium
bounds_dsed = [  0.26 0.5 1.0 2.0 5.0];    % Grain size mm  (min = 0.12 mm)    % this is only used to label output
dsed_states = {'fine' ;     'medium' ; 'coarse' ; 'verycoarse' ; 'gravel' }    % States in BN
dsedstr = char(dsed_states(find(dsed <= bounds_dsed, 1)))
dsedmm = dsed/1000;

outfilename = ['mcscour_h' num2str(round(Waterdepth)) 'm-' dsedstr '_' UXO.type ...    % self-documenting file name
                        'Sg' num2str(UXO.Sg*10) 'D' num2str(floor(UXO.Diam*100)) ]
fid = fopen([ outfilename 'cm.txt'],'w');
fixed_string = strjoin( {  [' ' num2str(Waterdepth)] , dsedstr , UXO.type }, '\t' );  % identify run; values used by
                                                                                       % Learn > Incorporate Case File
header = strjoin( { ' Hsig', 'T', 'Uc', 'alpha', 'beta', 'SB', 'h', 'dsed', 'UXO'  }, '\t' );
fprintf(fid, '%s \n', header);

TidalAmp_range = [0.0,  1.0] ; % m/s   Set appropriate to site of interest; may adjust to each spatial province
```

```
Hsig.range = [0.2, 8.0] ;       % m     Significant Wave Height drawn from Lognormal distribution
  Hsig.mu = -0.1;               %       mu & sig chosen based on regional wave climatology
  Hsig.sig = 0.66;              %       ( shown here: ~GoM analysis from Buoy 42029)
Period.range = [2 12];          % seconds  Draw from Normal distribution
  Period.mean = 5.7;            %          Again, based on regional wave climatology
  Period.sigma = 1.5;           % Future improvement would allow use of empirical joint PDF(Hsig, Period)

nvec = 999;  % each call to the Scour subroutine will compute nvec cases

% State bounds for angle bins in BN are 0 20 50 90 degrees for "parallel"  "angled"  and "perpendicular"
wc_angle_beta = [ 5 10 35 70 89];  % loop thru current parallel with wave, at angle, and perpendicular
alpha = [ 10 35 70 80 89  ];        % Angles here represent evidence that UXO likely to be --> perp;
nalpha = numel(alpha);

 for ibeta = 1:numel(wc_angle_beta)
      beta = wc_angle_beta(ibeta);

    for isamp =1:999    % many samples in this Monte Carlo exercise for each beta
        Hs = lognrnd(Hsig.mu,Hsig.sig , nvec,1);      % from Lognormal distrib
         mtoosmall = find(Hs < Hsig.range(1));         % replace too small with large values (which were undersampled)
         Hs(mtoosmall) = random('unif', Hsig.range(2)-3, Hsig.range(2), numel(mtoosmall),1);
         Hs(Hs > Hsig.range(2)) = Hsig.range(2);
        Tperiod =  random('norm', Period.mean, Period.sigma , nvec,1); % from  normal distrib
         Tperiod(Tperiod<Period.range(1)) = Period.range(1);
         Tperiod(Tperiod>Period.range(2)) = Period.range(2);
        tide_amp = random('unif',TidalAmp_range(1),TidalAmp_range(2) , nvec,1) ;  % from uniform distrib

       [ B ] = equilib_scourmc_fluidize_DemoVersion( Hs, Tperiod, tide_amp, UXO, Waterdepth,dsedmm, alpha, beta );
                 % note: beta is a scalar, alpha is an independent vector
                 % (This approach chosen to speed up MC exploration)
        for jj = 1:nvec
           for aa = 1:nalpha   % each input value is repeated numel(alpha) times
              fprintf(fid,  '%4.1f\t %4.1f\t %5.2f\t  %d\t %d\t  %5.2f\t %s\n',...
                  Hs(jj), Tperiod(jj), tide_amp(jj), alpha(aa), beta, B( ((jj-1)*nalpha)+aa ), fixed_string );
           end
        end

    end; % mc draw
 end ; % beta loop
 fclose(fid);

  %% save info to document choices for this Monte Carlo run
  save(outfilename, 'outfilename','fixed_string', 'Waterdepth', 'UXO','dsed', 'Hsig','Period')
```

*** end mc_scour_DemoVersion **********

*** mc_migrate_DemoVersion **********

```
%  mc_migrate_DemoVersion   April-June 2019   Script for Monte Carlo exploration of
%  Onset of mobility model plus adhoc migration distance estimation for UnMES.
%  Version where a UnMES Bayesian Network (BN)is built for each fixed spatial province (may be
%  a single grid cell) therefore  WaterDepth and Sediment Grain Size are
%  specified as scalar values.

%  UXO type is a structure, with separate output file written for each UXO type
%  for pratical purposes to constrain output file size. Written out in Ascii columns
%   which is directly readable with Netica's Learn > Incorporate Case File
%    S. E. Rennie    JHU/APL   June 2017
%    2017 version does not have alpha factor yet in onset of motion

addpath('/Users/rennise1/Documents/My Documents/MyNewWorkMac/SERDP/SERDPmatlab')

UXO.type = 'Lultra';  % Single UXO type set  for each run of this script
UXO.Sg   = 3.84;      % specific gravity
UXO.Diam = 0.14;      % meters    D = 25mm for bullet, 81mm for Mortar and 155mm for Howitzer

Waterdepth = 2.6;   % fixed for each run of this script
dsed       = 0.6 ;  % mm   0.25 fine sand for 7.5 & 20 m    0.4m medium for depth = 3m based on NAVO Bottom Sediment
Type map
bounds_dsed = [  0.26 0.5 1.0 2.0 5.0];    % Grain size mm  (min = 0.12 mm)    % this is only used to label output
dsed_states = {'fine' ;     'medium' ; 'coarse' ; 'verycoarse' ; 'pebbles' } ; % sediment States in BN
dsedstr = char(dsed_states(find(dsed < bounds_dsed, 1)))
dsedmm = dsed/1000;

outfilename = ['mcmigrate_h' num2str(round(Waterdepth)) 'm-' dsedstr '_' UXO.type ...
                          'Sg' num2str(UXO.Sg*10) 'D' num2str(floor(UXO.Diam*100)) ]
fid = fopen( [outfilename 'cm.txt'],'w');
fixed_string = strjoin( {  [' ' num2str(Waterdepth)] , dsedstr , UXO.type }, '\t' ); % identify run; values used by
                                                                                      % Learn > Incorporate Case File

header = strjoin( { ' Hsig', 'T', 'Uc',  'beta', 'SB', 'Mdist', 'h', 'dsed', 'UXO'  }, '\t' );
                                                        % Note No alpha factor yet for motion
fprintf(fid, '%s \n', header);

TidalAmp_range = [0.0,  1.0] ; % m/s   Set appropriate to site of interest; may adjust to each spatial province
SB_range = [0.0,  1.1] ;       % Scour ( & Fluidize  Burial  Range
Hsig.range = [0.2, 8.0] ;      % m     Significant Wave Height drawn from Lognormal distribution
  Hsig.mu = -0.1;              %       mu & sig chosen based on regional wave climatology
  Hsig.sig = 0.66;             %       ( shown here: ~GoM analysis from Buoy 42029)
Period.range = [2 12];         % seconds  Draw from Normal distribution
  Period.mean = 5.7;           %          Again, based on regional wave climatology
  Period.sigma = 1.5;          % Future improvement would allow use of empirical joint PDF(Hsig, Period)
```

```
nvec = 999;  % each call to the migrate subroutine will compute nvec cases

% State bounds for angle bins are 0 20 50 90 degrees for "parallel"  "angled"  and "perpendicular"
wc_angle_beta = [ 5 10  35 70  89] ; % loop thru current parallel with wave, at angle and perpendicular

 for ibeta = 1:numel(wc_angle_beta)
      beta = wc_angle_beta(ibeta);

    for isamp =1:1999    % many many samples in this Monte Carlo simulation

        Hs = lognrnd(Hsig.mu,Hsig.sig , nvec,1) ;  % from Lognormal distrib
           mtoosmall = find(Hs < Hsig.range(1));   % replace too small with large values (which were undersampled)
           Hs(mtoosmall) = random('unif', Hsig.range(2)-3, Hsig.range(2), numel(mtoosmall),1) ;
           Hs(Hs > Hsig.range(2)) = Hsig.range(2) ;
        Tperiod =  random('norm', Period.mean, Period.sigma , nvec,1)  % from  normal distrib
           Tperiod(Tperiod<Period.range(1)) = Period.range(1);
           Tperiod(Tperiod>Period.range(2)) = Period.range(2);
        tide_amp = random('unif',TidalAmp_range(1),TidalAmp_range(2) , nvec,1) ;  % from uniform distrib
        SB = random('unif',SB_range(1),SB_range(2) , nvec,1) ;  % from uniform distrib

       [ Mdist ] = mobility_migrate_DemoVersion( Hs, Tperiod, tide_amp, UXO, Waterdepth,dsedmm, SB, beta );

        for jj = 1:nvec
              fprintf(fid,  '%4.1f\t %4.1f\t %5.2f\t  %d\t %5.2f\t  %6.1f\t %s\n',...
                      Hs(jj), Tperiod(jj), tide_amp(jj), beta, SB(jj), Mdist(jj), fixed_string );
        end

    end; % mc draw
 end ; % beta loop
 fclose(fid);
  %% save info to document choices for this Monte Carlo run
  save(outfilename, 'outfilename','fixed_string', 'Waterdepth', 'UXO','dsed', 'Hsig','Period', …
       'SB_range', 'TidalAmp_range')
```

*** end mc_migrate_DemoVersion **********

*** equilib_scourmc_fluidize_DemoVersion **********

```
function [ B ] = equilib_scourmc_fluidize_DemoVersion( Hs, Tperiod, Uc, UXO, Waterdepth,dsed, alpha, beta )
% Compute equilibrium scour burial under combined waves and currents.
% implementing euqations from Friedrichs et al [2016]  Self-Burial paper [2016] ICSE (CRC Press)
% Also include Fluidization process estimate (adhoc Dec 2016) if Shield # > 1.0 (or breaking waves)
%
% Input  (each can be scalar or vector)
%   Hs          Signifcant wave height (m)  (scalar or vector)
%   Tperiod     Period of waves (s)         (scalar or vector)
%   Uc          current speed (average over water column?  representative of mid-depth?

%   UXO         structure describing munition  single structure applies to  all elements in vector
%   Waterdepth  depth at this location (m)  (scalar or vector)
%   dsed        median sediment grain size (m) (scalar or vector)  Note: in meters
%               UXO.type is string with name
%               UXO.Sg is specific gravity
%               UXO.Diam is diameter (m)

%   alpha  angle of attack -- angle (deg) between UXO long axis and orbital  wave direction (0 = parallel)
%   ^^^  alpha  can be vector even when Hs, T, Uc are scalars <-- allows efficient MC computation
%         If alpha vector of a different length than Hs, will be swept thru using repeated Hs,etc values
%   beta        angle (deg) between current and orbital wave velocity direction (0 = parallel)
%   ^^^^  but beta must be either scalar, or same vector length as Hs
% Output  (same length as Hsig or alpha, whichever is longer, or numel(Hsig)*numel(alpha) )
%   B    fractional equilibrium scour burial  = BurialDepth/Diam
    g = 9.81;       % gravity m/s/s
    kappa = 0.41;   % Von Karman's constant
    TE = 15;        % represntative Temperature deg C.
    nu = 1.79e-6./(1 + 0.03368*TE + 0.00021*TE.^2);  % viscosity of water

   hflag=1;   % means Hsig not Hrms
 [ UwHsig, waveLength, flagBreak] = bottom_orbital_vel(Hs, Tperiod, Waterdepth, hflag);

   %%%%%%%% u_star for currents from Garcia (2008) presentation of Yalin (1992) %%%%%%
    Zobs = Waterdepth/2;   % assume Uc is representative of mid-depth
    kb = 2.5*dsed;
    u_starc=0.01 ;  % initial guess
    for j=1:10
        Res=u_starc.*kb/nu;  % roughness Reynolds #
```

```
        Bs=8.5 + ((1/kappa)*log(Res)-3) .* (exp(-0.121 * (log(Res)).^2.42)) ;  % Eq. 29-b in Garcia 2008
        u_starc=Uc./((1/kappa)*log(Zobs./kb)+Bs); % in meters/sec
    end
    UcD=real(u_starc .* ((1/kappa).*log(UXO.Diam./kb)+Bs) ); % Uc at top of object
    %      Shieldc=(u_starc.^2)./(g*1.65*dsed);   % Not used in this version
    %      fwC=2*(u_starc./UcD).^2;               % Retain for possible future use  if Uc >> Uw ??

    Um = sqrt( UwHsig.^2 + UcD.^2 + 2.*UwHsig.*UcD.*abs(cosd(beta))); % Eq7 in Friedrichs et al.[2016]

% compute SedShields & KC  using Friedrichs's equations from ICSE Scour paper 2016
% Strictly, this should be for when Uw >> Uc
% However note that friction factor for current would be much smaller    fwC < fw

    KC = Um.*Tperiod./UXO.Diam;     % Keulegan-Carpenter number

    A=Tperiod.*Um/(2*pi);  % amplitude of wave orbital excursion
    Rew=Um.*A/nu;    % wave Reynolds #  Rw
    sqf=.05;         % initial guess for sqrt(fw)
    Rakf=Rew.*sqf./(A./kb);
    for j=1:10;
        RHS=log(6.36*(A./kb).*sqf)-log(1-exp(-0.0262*Rakf)+4.71./Rakf);
        RHS=RHS.^2+1.64;
        fw=(0.32)./RHS;    % see Eq 6 in Friedrichs, et al. [2016]; also Demir&Garcia Eq.(13)
        sqf=sqrt(fw);      % new estimate of fw
        Rakf=Rew.*sqf./(A./kb);
    end
    fw(fw > 0.0414) = 0.0414 ; % following bound applied in Swart 1974
    Shieldw=0.5*fw.*(Um.^2)./(g*1.65*dsed);

% adjust for ratio of Current to Total bottom flow Fig. 8(a) in Friedrichs et al 2016
%  Cataño-Lopera [2011] B/D  found to decrease as Uc||/Um increased
%  i.e LESS burial observed if currents are a larger contribution to combined Um
    UcUm = UcD.*abs(cosd(beta))./Um ; % only count component of current that is parallel to waves
    fUCpar = exp(-1.1*UcUm);          % for combined currents and waves
    fUCpar(fUCpar<0.6) = 0.6;          % bound correction for currents to approx ~ Uc >= Uw

%  adjust for alpha angle of UXO long axis to wave orbital vel as proposed in Friedrichs et al 2016.
%  See Fig 8(b) f(alpha) = exp(-3.4*(cos(alpha)-0.6)*UcUm)  But ONLY for
%  alpha such that cos(alpha) = 0.6 --> alpha = 53 deg
    falpha = exp(-2.5*(cosd(alpha)-0.6)) ;    % Note updated exponent based on more reasonable fit.
    mperp = find(cosd(alpha) <= 0.6) ;        % Find the times when current is mostly perpedicular.
    falpha(mperp) = 1.0 ;                     % Bound for "perpendicular"
```

```
% summary burial equation Friedrich's equations cylinders under waves+current
% See Figures Fig.7 & Fig. 9 in Friedrichs et al., Self Burial by Scour ICSE 2016
 fS = (1.85* Shieldw.^0.34);
 fKC = 0.1.*KC.^0.51 ;

  if numel(alpha) ~= numel(Hs)  % allow repetition thru numel(alpha) for speed
     BSKCUc =  ((fS(:) .* fKC(:)) .*fUCpar(:) * falpha)';
     B = BSKCUc(:);
     flagBreak_alpha =  (flagBreak(:) * ones(size(falpha)))';  % expand other vector
     flagBreak = flagBreak_alpha(:);
     Shieldw_alpha =   (Shieldw(:) * ones(size(falpha)))';   % to test for high-energy conditions
     Shieldw = Shieldw_alpha(:);
  else
    B = fS .*falpha .* fUCpar .* fKC ;
  end
  B( B> 1.15) = 1.15;  % cap at maximum scour depth

 % overwrite values if high-energy FLUIDIZATION conditions occurred:

   mBreak = find( flagBreak > 0 ); % breaking due to shallow depth or steepness
   B(mBreak) = fluidize_estimate_DemoVersion(UXO); % when breaking, assume complete fluidization for now

   msheet = find(Shieldw > 0.7); % sheet flow conditions --> fluidization
   B(msheet) = fluidize_estimate_DemoVersion(UXO);
end
```

*** end equilib_scourmc_fluidize_DemoVersion **********

*** mobility_migrate_DemoVersion **********

```
function [ Mdist  ] = mobility_migrate_DemoVersion( Hs, Tperiod, Uc, UXO, Waterdepth,dsed, SB, beta )
% Given an estimate for fractional burial, predict onset of mobility.
% Estimate migration distance in rule-of-thumb manner based on mobility
% number exceedance over threshold.
%
% Input  (each can be scalar or vector)
%   Hs          Significant wave height (m)  (scalar or vector)  !!! Note: U10 will be computed !!
%   Tperiod     Period of waves (s)         (scalar or vector)
%   Uc          current speed (average over water column -->  representative of mid-depth)
%   UXO         structure describing munition (single structure applies to all elements in Hs vector)
%               UXO.type is string with name
%               UXO.Sg is specific gravity
%               UXO.Diam is diameter (m)
%   Waterdepth  depth at this location (m)  (scalar or vector)
%   dsed        median sediment grain size (m) (scalar or vector)  Note: in meters
%   SB          fractional equilibrium scour burial BurialDepth/Diam (will function as kbed)

%   beta        angle (deg) between current and orbital wave velocity direction (0 = parallel)
%   ^^^^   beta must be either scalar, or same vector length as Hs
%   Not used yet: alpha  angle of attack -- Factor for mobility not included in Spring 2017 version
%
% Output  (same length as Hsig  )
%   Mdist      migration distance in meters (same size as Hs)
%
%  S. E. Rennie   JHUAPL May-June 2017
    g = 9.81;       % gravity m/s/s
    kappa = 0.41;   % Von Karman's constant
    TE = 15;        % represntative Temperature deg C.
    nu = 1.79e-6./(1 + 0.03368*TE + 0.00021*TE.^2);  % viscosity of water

  hflag=10;   % means return bot.vel for U10, highest 10% of wave heights
  [ UwH10, waveLength, flagBreak] = bottom_orbital_vel(Hs, Tperiod, Waterdepth, hflag);

   %%%%%%%% u_star for currents from Garcia (2008) presentation of Yalin (1992) %%%%%%
    Zobs = Waterdepth/2;   % assume Uc is representative of mid-depth
    kb = 2.5*dsed;
    u_starc=0.01 ;  % initial guess
    for j=1:10
        Res=u_starc.*kb/nu;  % roughness Reynolds #
```

```
        Bs=8.5 + ((1/kappa)*log(Res)-3) .* (exp(-0.121 * (log(Res)).^2.42)) ;  % Eq. 29-b in Garcia 2008
        u_starc=Uc./((1/kappa)*log(Zobs./kb)+Bs); % in meters/sec
    end
    UcD=real(u_starc .* ((1/kappa).*log(UXO.Diam./kb)+Bs) ); % Uc at top of object

    Um = sqrt( UwH10.^2 + UcD.^2 + 2.*UwH10.*UcD.*abs(cosd(beta))); % Eq 7 Friedrich et al.[2016] ICSE

    A=Tperiod.*Um/(2*pi);  % amplitude of wave orbital excursion
    Rew=Um.*A/nu;           % wave Reynolds #  Rw
    sqf=.05;                % initial guess for sqrt(fw)
    Rakf=Rew.*sqf./(A./kb);
    for j=1:10;
        RHS=log(6.36*(A./kb).*sqf)-log(1-exp(-0.0262*Rakf)+4.71./Rakf);
        RHS=RHS.^2+1.64;
        fw=(0.32)./RHS;    % see Eq 6 in Friedrichs, Rennie, Brandt [2016] also Demir&Garcia Eq.(13)
        sqf=sqrt(fw);      % new estimate of fw
        Rakf=Rew.*sqf./(A./kb);
    end
    fw(fw > 0.0414) = 0.0414 ; % following bound applied in Swart 1974
    Shieldw=0.5*fw.*(Um.^2)./(g*1.65*dsed);

    kbed = SB.*0.0 + 2.5*dsed ;      % nominal bed roughness if no burial
                                     % (Potentially in future version, ripple height could be important)
    BurialDepth = SB .* UXO.Diam;    % SB is fractional burial.  Make dimensional (meters)
    mburied = BurialDepth > kbed;    % (these will be likely almost ALL )
    kbed(mburied) = BurialDepth(mburied);
    DratioK = UXO.Diam ./ kbed;
    DratioK(DratioK > 300) = 300;  % limit the Diameter to bottom roughness effect (flat for large D/kbed)

    %  Empirical  Fit for parameters as published in Rennie, Brandt & Friedrich OceanEngineering 2017
    acrit_fit = 1.64;  bcrit_fit = -0.71;         % Best fit to Critical Mobility # as function of D/k
    Qobj_crit = acrit_fit*(DratioK).^bcrit_fit ;  % threshold
    %      alo = 1.5164 ;   blo = -0.7361;  % 95% cond. interval not used in monte carlo simulation
    %      ahi = 1.7709  ;  bhi = -0.6872;
    %      Qcritlo = alo*(DratioK).^blo ;
    %      Qcrithi = ahi*(DratioK).^bhi ;
     denom = g.*( UXO.Sg - 1).*UXO.Diam ;  % denominator of Mobility number
     Mobnum = Um.^2./denom;                % Mobility number Qobj   Not yet corrected for inertial effects

    KC = Um.*Tperiod./UXO.Diam;  % Keulegan-Carpenter number becomes small for short-period waves
                                 %  or larger diam UXO.  KC --> large means steady flow
% since fI is unbounded as KC--> 0; impose a reasonable limit to this factor so that Ucrit does not -> 0
```

```
        KC(KC < 5) = 5;    % this bounds fI to 5.1X which is still a substantial correction
    fI = sqrt(1+16*pi^2*4*KC.^(-2));   % Inertial force correction for oscillatory flow
                                        %[see Eq(10) OceanEngineering 2017 ]
         % fI is a significant correction (>2X)for KC < 15.  fI --> 1 for Large KC (steady flow).

    Mobnum_fI = Mobnum.*fI;      %  effective Mob # including inertial contribution from Waves
    Mdist =  migrate_estimate_DemoVersion(Mobnum_fI, Qobj_crit, Um, Tperiod);

  % Suggested mobility behavior: "Lockdown" for burial greater than some value, no matter the forcing
   mBury = find( SB > 0.9 );  %overwrite migration values if TOO deep burial, here set to 90%
   Mdist(mBury) = 0.0;
end
```

*** end mobility_migrate_DemoVersion ***********

Appendix B: Matlab code to perform rule of thumb estimation.

```
***   fluidize_estimate_DemoVersion  **********

function BF =  fluidize_estimate_DemoVersion(UXO)
% assuming sheet flow conditions, estimate burial using ad-hoc formula based
% on combined lab and Field data sets from J. Calantoni (2015, 2016),
% lab data from Catano-Lopera et al. [2007]  and field data from
% P. Traykovski (Long Point, 2015).
% Input is single UXO structure with specific gravity in field UXO.Sg.
% Output is scalar BF meaning fractional burial (BurialDepth/Diameter)
% Estimate of fractional burial due to fluidization is determined by random
% draw into a uniform distribution with a range determined by
% the ratio of UXO density,to sediment grain density.
% S. E. Rennie JHU/APL   April 2017

Rho_sediment = 2.65;  % use grain density of quartz
ratio = UXO.Sg/Rho_sediment;   % all scalar
slope = 3.8 ; % this top slope is  ad hoc
BFrangeTop = min([ max([(slope*ratio-(slope*0.82)), 0]) , 2] );

slope =0.76 ; % this bottom slope is also ad hoc
BFrangeBottom = min([ max([(slope*ratio-(slope*1.06)), 0]) , 2] );

BF = random('unif', BFrangeBottom, BFrangeTop ) ;
% Note that maximum "fluidized" burial is fixed at twice the UXO diameter
end

*** end fluidize_estimate_DemoVersion  **********
```

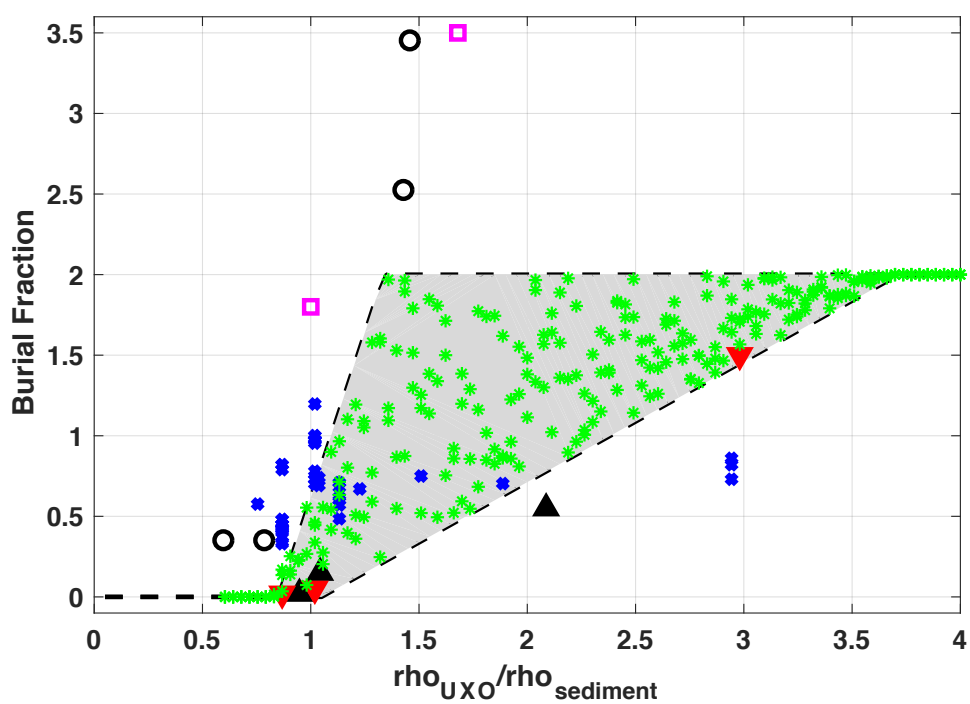

Figure B.1 Diagram showing ad hoc estimate of burial fraction (green stars) due to fluidization as random function of ratio of UXO density to sand grain density overlaid on plot as from Figure 2.1

*** migrate_estimate_DemoVersion **********

Migration Distance is currently estimated with a rule-of-thumb approach where distance is assumed to be a function of Θ_{obj} exceedance over Θ_{obj_crit}. The algorithm to construct the CPT has been adjusted to reflect the results from the Long Point field experiment (blue points in Figure B.2) where migration distances of tens of meters were measured for mobility number larger than, but still the same order of magnitude as Θ_{obj_crit}. However, the Long Point data do not exhibit significant dependence on mobility number exceedance, emphasizing the need for further research and understanding into migration phenomenology. The estimation procedure documented here should be considered a placeholder for a future improved model.

```
function Mdist = migrate_estimate_DemoVersion(Sobj, Sthreshold, Ubot, Twave)
%  AD HOC version of migration distance estimate based on exceedance of
% Mobility # over threshold.
% Notes from 2017 ad hoc implementation:
% 1) if Sobj is > Sthreshold  but not twice as big, then think of UXO as
%    rolling along the bottom for ½ of some number of  wave periods
%    ([Davis et al., 2007 : rolling cylinders travel at 70% of Ubot)
% 2) if Sobj is > 2XSthreshold think of it as "blowing" away (100% of Ubot)
   Sratio = Sobj./Sthreshold;
   Mdist = 7*(Sratio-1).^0.3.* Ubot.*0.5.*Twave;  % ad hoc scaling of 100% of
                    %Ubot for 1/2 the wave period for f(Sratio-1) # of waves
   mm = find(Sratio < 3);
   Mdist(mm) = 0.7.*Ubot(mm).*0.5.*Twave(mm).*(Sratio(mm).^1.8 -1)*1.9;
   mm = find(Sratio < 1);
   Mdist(mm) = 0.0; %  below threshold, no movement
   Mdist(Mdist>999) = 999;  % impose limit matching UnMES bin max Spring 2017
 end
```

*** end migrate_estimate_DemoVersion **********

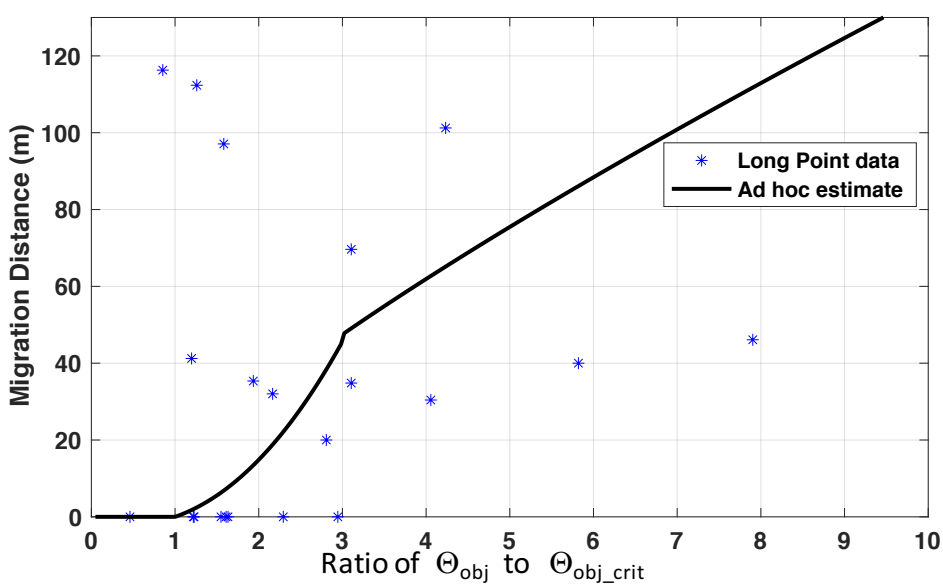

Figure B.2 Plot of observed and estimated migration distance as a function of mobility number ratio to the critical threshold from onset of motion.

Appendix C: Example Conditional Probability Table (CPT)

Shown below in Table C.1 are portions of the CPT defining UXO migration dependence on waves and currents in the Netica implementation of a UnMES Demonstration Version BN. In addition to the hydrodynamic forcing, parent nodes are the UXO type (which defines the density) and the fractional burial. The migration distances are computed in a Monte Carlo (MC) simulation using the code shown in Appendices A & B, and the MC output incorporated into Netica as a file of cases. Parameter learning of CPTs in Netica from cases is computed with a counting-learning approach, which, although simple, is a true Bayesian learning algorithm [Norsys, 2017]. Before learning begins, the node starts off in a state of ignorance, i.e., probabilities are uniform, and each experience is set to 1.

The Migration Distance node has 3 states, with distance discretized into "Stay" (0 to 5 m), "Near" (5 to 50 m), and "Far" (more than 50 m). The wave nodes for Height and Period have 11 and 4 states, respectively, in this implementation. Tidal current can take on any of 6 levels, and the wave-current angle β (see Section 2.3.1) is described as either parallel, angled, or perpendicular. As in Section 3.3, burial falls in one of 5 states; the burial state labeled "perc20to50" was set to represent the range of partial burial predicted by the time-dependent application of the burial process model. The resulting CPT for Migration Distance then has almost 4000 entries for each UXO type. The CPT sections in Table C.1 show example migration probabilities for all four of the surrogate UXO used in the 2015 field experiment at Long Point [Traykovski & Austin, 2017], which are enumerated in the "UXO type" node shown in Figure C.1. The BN was generated for a water depth of 3 m and sand grain size 0.6 mm. In order to understand and verify the BN prediction behavior, the "UXO type" state is set 100% to a single UXO (Figures C.1 and 3.5). However, in an operational application a distribution of UXO types might be of most interest to the site manager.

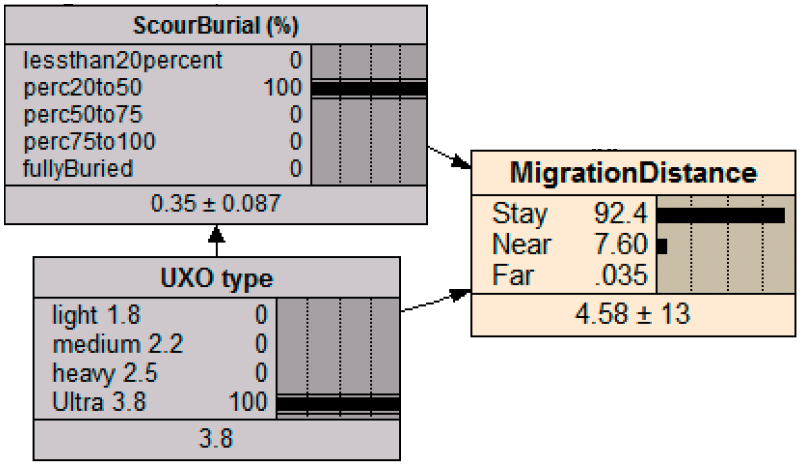

Figure C.1 Nodes from UnMES BN representing migration distance prediction for partially buried UXO with specific gravity 3.8, given wave distribution centered about state 1.7 to 2 m height.

Table C.1 Sections of Conditional Probability Table for Migration Distance

UXO type	WaveHeight (m)	TidalCurrent (m/s)	Period (s)	Wave-Current angle	Scour | Fluidize	Stay	Near	Far
light 1.8	1.4 to 1.7	0 to 0.1	2 to 4	parallel	lessthan20percent	10.182	76	13.818
light 1.8	1.4 to 1.7	0 to 0.1	2 to 4	parallel	perc20to50	79.024	20.732	0.244
light 1.8	1.4 to 1.7	0 to 0.1	2 to 4	parallel	perc50to75	99.432	0.284	0.284
light 1.8	1.4 to 1.7	0 to 0.1	2 to 4	parallel	perc75to100	99.459	0.27	0.27
light 1.8	1.4 to 1.7	0 to 0.1	2 to 4	parallel	fullyBuried	98.551	0.725	0.725
light 1.8	1.4 to 1.7	0 to 0.1	2 to 4	angled	lessthan20percent	11.198	77.8	11.002
light 1.8	1.4 to 1.7	0 to 0.1	2 to 4	angled	perc20to50	79.427	20.443	0.13
light 1.8	1.4 to 1.7	0 to 0.1	2 to 4	angled	perc50to75	99.686	0.157	0.157
light 1.8	1.4 to 1.7	0 to 0.1	2 to 4	angled	perc75to100	99.696	0.152	0.152
light 1.8	1.4 to 1.7	0 to 0.1	2 to 4	angled	fullyBuried	99.315	0.342	0.342
light 1.8	1.4 to 1.7	0 to 0.1	2 to 4	perpendicular	lessthan20percent	15.464	74.742	9.794
light 1.8	1.4 to 1.7	0 to 0.1	2 to 4	perpendicular	perc20to50	81.457	18.46	0.0828
light 1.8	1.4 to 1.7	0 to 0.1	2 to 4	perpendicular	perc50to75	99.796	0.102	0.102
light 1.8	1.4 to 1.7	0 to 0.1	2 to 4	perpendicular	perc75to100	99.798	0.101	0.101
light 1.8	1.4 to 1.7	0 to 0.1	2 to 4	perpendicular	fullyBuried	99.54	0.23	0.23
light 1.8	1.4 to 1.7	0 to 0.1	4 to 6	parallel	lessthan20percent	0.105	58.421	41.474
light 1.8	1.4 to 1.7	0 to 0.1	4 to 6	parallel	perc20to50	20.652	79.28	0.0679
light 1.8	1.4 to 1.7	0 to 0.1	4 to 6	parallel	perc50to75	92.152	7.767	0.0809
light 1.8	1.4 to 1.7	0 to 0.1	4 to 6	parallel	perc75to100	99.835	0.0824	0.0824
light 1.8	1.4 to 1.7	0 to 0.1	4 to 6	parallel	fullyBuried	99.621	0.189	0.189
light 1.8	1.4 to 1.7	0 to 0.1	4 to 6	angled	lessthan20percent	0.0526	62.316	37.632
light 1.8	1.4 to 1.7	0 to 0.1	4 to 6	angled	perc20to50	25.137	74.829	0.0342
light 1.8	1.4 to 1.7	0 to 0.1	4 to 6	angled	perc50to75	94.857	5.101	0.0422
light 1.8	1.4 to 1.7	0 to 0.1	4 to 6	angled	perc75to100	99.919	0.0407	0.0407
light 1.8	1.4 to 1.7	0 to 0.1	4 to 6	angled	fullyBuried	99.797	0.102	0.102
light 1.8	1.4 to 1.7	0 to 0.1	4 to 6	perpendicular	lessthan20percent	0.0351	62.811	37.154
light 1.8	1.4 to 1.7	0 to 0.1	4 to 6	perpendicular	perc20to50	28.374	71.604	0.0223
light 1.8	1.4 to 1.7	0 to 0.1	4 to 6	perpendicular	perc50to75	96.091	3.882	0.0273
light 1.8	1.4 to 1.7	0 to 0.1	4 to 6	perpendicular	perc75to100	99.943	0.0285	0.0285
light 1.8	1.4 to 1.7	0 to 0.1	4 to 6	perpendicular	fullyBuried	99.862	0.0688	0.0688

UXO type	WaveHeight (m)	TidalCurrent (m/s)	Period (s)	Wave-Current angle	Scour | Fluidize	Stay	Near	Far
medium 2.2	1.7 to 2	0 to 0.1	2 to 4	parallel	lessthan20percent	15.232	69.536	15.232
medium 2.2	1.7 to 2	0 to 0.1	2 to 4	parallel	perc20to50	85.124	14.463	0.413
medium 2.2	1.7 to 2	0 to 0.1	2 to 4	parallel	perc50to75	99.029	0.485	0.485
medium 2.2	1.7 to 2	0 to 0.1	2 to 4	parallel	perc75to100	99.134	0.433	0.433
medium 2.2	1.7 to 2	0 to 0.1	2 to 4	parallel	fullyBuried	97.647	1.176	1.176
medium 2.2	1.7 to 2	0 to 0.1	2 to 4	angled	lessthan20percent	18.678	67.529	13.793
medium 2.2	1.7 to 2	0 to 0.1	2 to 4	angled	perc20to50	85.236	14.567	0.197
medium 2.2	1.7 to 2	0 to 0.1	2 to 4	angled	perc50to75	99.497	0.251	0.251
medium 2.2	1.7 to 2	0 to 0.1	2 to 4	angled	perc75to100	99.534	0.233	0.233
medium 2.2	1.7 to 2	0 to 0.1	2 to 4	angled	fullyBuried	98.919	0.541	0.541
medium 2.2	1.7 to 2	0 to 0.1	2 to 4	perpendicular	lessthan20percent	15.866	69.311	14.823
medium 2.2	1.7 to 2	0 to 0.1	2 to 4	perpendicular	perc20to50	86.308	13.57	0.122
medium 2.2	1.7 to 2	0 to 0.1	2 to 4	perpendicular	perc50to75	99.691	0.154	0.154
medium 2.2	1.7 to 2	0 to 0.1	2 to 4	perpendicular	perc75to100	99.672	0.164	0.164
medium 2.2	1.7 to 2	0 to 0.1	2 to 4	perpendicular	fullyBuried	99.291	0.355	0.355
medium 2.2	1.7 to 2	0 to 0.1	4 to 6	parallel	lessthan20percent	0.165	59.241	40.594
medium 2.2	1.7 to 2	0 to 0.1	4 to 6	parallel	perc20to50	26.251	73.647	0.102
medium 2.2	1.7 to 2	0 to 0.1	4 to 6	parallel	perc50to75	96.401	3.47	0.129
medium 2.2	1.7 to 2	0 to 0.1	4 to 6	parallel	perc75to100	99.745	0.127	0.127
medium 2.2	1.7 to 2	0 to 0.1	4 to 6	parallel	fullyBuried	99.408	0.296	0.296
medium 2.2	1.7 to 2	0 to 0.1	4 to 6	angled	lessthan20percent	0.0831	60.183	39.734
medium 2.2	1.7 to 2	0 to 0.1	4 to 6	angled	perc20to50	29.077	70.869	0.0536
medium 2.2	1.7 to 2	0 to 0.1	4 to 6	angled	perc50to75	97.49	2.444	0.0661
medium 2.2	1.7 to 2	0 to 0.1	4 to 6	angled	perc75to100	99.872	0.0639	0.0639
medium 2.2	1.7 to 2	0 to 0.1	4 to 6	angled	fullyBuried	99.702	0.149	0.149
medium 2.2	1.7 to 2	0 to 0.1	4 to 6	perpendicular	lessthan20percent	0.0554	59.645	40.299
medium 2.2	1.7 to 2	0 to 0.1	4 to 6	perpendicular	perc20to50	34.495	65.469	0.0356
medium 2.2	1.7 to 2	0 to 0.1	4 to 6	perpendicular	perc50to75	98.526	1.432	0.0421
medium 2.2	1.7 to 2	0 to 0.1	4 to 6	perpendicular	perc75to100	99.917	0.0416	0.0416
medium 2.2	1.7 to 2	0 to 0.1	4 to 6	perpendicular	fullyBuried	99.791	0.105	0.105

Table C.1 Sections of Conditional Probability Table for Migration Distance (cont.)

UXO type	WaveHeight (m)	TidalCurrent (m/s)	Period (s)	Wave-Current angle	Scour | Fluidize	Stay	Near	Far
heavy 2.5	2 to 2.5	0 to 0.1	2 to 4	parallel	lessthan20percent	10.811	68.649	20.541
heavy 2.5	2 to 2.5	0 to 0.1	2 to 4	parallel	perc20to50	74.708	24.903	0.389
heavy 2.5	2 to 2.5	0 to 0.1	2 to 4	parallel	perc50to75	99.029	0.485	0.485
heavy 2.5	2 to 2.5	0 to 0.1	2 to 4	parallel	perc75to100	99.02	0.49	0.49
heavy 2.5	2 to 2.5	0 to 0.1	2 to 4	parallel	fullyBuried	97.98	1.01	1.01
heavy 2.5	2 to 2.5	0 to 0.1	2 to 4	angled	lessthan20percent	14.804	71.903	13.293
heavy 2.5	2 to 2.5	0 to 0.1	2 to 4	angled	perc20to50	77.645	22.156	0.2
heavy 2.5	2 to 2.5	0 to 0.1	2 to 4	angled	perc50to75	99.528	0.236	0.236
heavy 2.5	2 to 2.5	0 to 0.1	2 to 4	angled	perc75to100	99.539	0.23	0.23
heavy 2.5	2 to 2.5	0 to 0.1	2 to 4	angled	fullyBuried	98.851	0.575	0.575
heavy 2.5	2 to 2.5	0 to 0.1	2 to 4	perpendicular	lessthan20percent	19.172	66.885	13.943
heavy 2.5	2 to 2.5	0 to 0.1	2 to 4	perpendicular	perc20to50	80.415	19.455	0.13
heavy 2.5	2 to 2.5	0 to 0.1	2 to 4	perpendicular	perc50to75	99.687	0.157	0.157
heavy 2.5	2 to 2.5	0 to 0.1	2 to 4	perpendicular	perc75to100	99.681	0.159	0.159
heavy 2.5	2 to 2.5	0 to 0.1	2 to 4	perpendicular	fullyBuried	99.231	0.385	0.385
heavy 2.5	2 to 2.5	0 to 0.1	4 to 6	parallel	lessthan20percent	0.172	43.225	56.604
heavy 2.5	2 to 2.5	0 to 0.1	4 to 6	parallel	perc20to50	17.647	82.246	0.107
heavy 2.5	2 to 2.5	0 to 0.1	4 to 6	parallel	perc50to75	83.2	16.667	0.133
heavy 2.5	2 to 2.5	0 to 0.1	4 to 6	parallel	perc75to100	99.321	0.543	0.136
heavy 2.5	2 to 2.5	0 to 0.1	4 to 6	parallel	fullyBuried	99.369	0.315	0.315
heavy 2.5	2 to 2.5	0 to 0.1	4 to 6	angled	lessthan20percent	0.0823	43.374	56.543
heavy 2.5	2 to 2.5	0 to 0.1	4 to 6	angled	perc20to50	17.599	82.182	0.219
heavy 2.5	2 to 2.5	0 to 0.1	4 to 6	angled	perc50to75	85.798	14.136	0.0654
heavy 2.5	2 to 2.5	0 to 0.1	4 to 6	angled	perc75to100	99.796	0.136	0.068
heavy 2.5	2 to 2.5	0 to 0.1	4 to 6	angled	fullyBuried	99.704	0.148	0.148
heavy 2.5	2 to 2.5	0 to 0.1	4 to 6	perpendicular	lessthan20percent	0.0554	46.341	53.603
heavy 2.5	2 to 2.5	0 to 0.1	4 to 6	perpendicular	perc20to50	21.336	78.592	0.0722
heavy 2.5	2 to 2.5	0 to 0.1	4 to 6	perpendicular	perc50to75	87.617	12.339	0.0445
heavy 2.5	2 to 2.5	0 to 0.1	4 to 6	perpendicular	perc75to100	99.912	0.0439	0.0439
heavy 2.5	2 to 2.5	0 to 0.1	4 to 6	perpendicular	fullyBuried	99.796	0.102	0.102

UXO type	WaveHeight (m)	TidalCurrent (m/s)	Period (s)	Wave-Current angle	ScourBurial (%)	Stay	Near	Far
Ultra 3.8	2.5 to 3	0 to 0.1	2 to 4	parallel	lessthan20percent	17.204	64.516	18.28
Ultra 3.8	2.5 to 3	0 to 0.1	2 to 4	parallel	perc20to50	91.071	8.036	0.893
Ultra 3.8	2.5 to 3	0 to 0.1	2 to 4	parallel	perc50to75	98.347	0.826	0.826
Ultra 3.8	2.5 to 3	0 to 0.1	2 to 4	parallel	perc75to100	98.148	0.926	0.926
Ultra 3.8	2.5 to 3	0 to 0.1	2 to 4	parallel	fullyBuried	95.745	2.128	2.128
Ultra 3.8	2.5 to 3	0 to 0.1	2 to 4	angled	lessthan20percent	20.93	65.116	13.953
Ultra 3.8	2.5 to 3	0 to 0.1	2 to 4	angled	perc20to50	92.8	6.8	0.4
Ultra 3.8	2.5 to 3	0 to 0.1	2 to 4	angled	perc50to75	99.065	0.467	0.467
Ultra 3.8	2.5 to 3	0 to 0.1	2 to 4	angled	perc75to100	99.087	0.457	0.457
Ultra 3.8	2.5 to 3	0 to 0.1	2 to 4	angled	fullyBuried	97.647	1.176	1.176
Ultra 3.8	2.5 to 3	0 to 0.1	2 to 4	perpendicular	lessthan20percent	21.132	60.755	18.113
Ultra 3.8	2.5 to 3	0 to 0.1	2 to 4	perpendicular	perc20to50	88.36	11.376	0.265
Ultra 3.8	2.5 to 3	0 to 0.1	2 to 4	perpendicular	perc50to75	99.317	0.341	0.341
Ultra 3.8	2.5 to 3	0 to 0.1	2 to 4	perpendicular	perc75to100	99.342	0.329	0.329
Ultra 3.8	2.5 to 3	0 to 0.1	2 to 4	perpendicular	fullyBuried	98.374	0.813	0.813
Ultra 3.8	2.5 to 3	0 to 0.1	4 to 6	parallel	lessthan20percent	0.324	42.718	56.958
Ultra 3.8	2.5 to 3	0 to 0.1	4 to 6	parallel	perc20to50	35.853	63.931	0.216
Ultra 3.8	2.5 to 3	0 to 0.1	4 to 6	parallel	perc50to75	96.85	2.887	0.262
Ultra 3.8	2.5 to 3	0 to 0.1	4 to 6	parallel	perc75to100	99.496	0.252	0.252
Ultra 3.8	2.5 to 3	0 to 0.1	4 to 6	parallel	fullyBuried	98.676	0.662	0.662
Ultra 3.8	2.5 to 3	0 to 0.1	4 to 6	angled	lessthan20percent	0.166	48.344	51.49
Ultra 3.8	2.5 to 3	0 to 0.1	4 to 6	angled	perc20to50	34.816	65.076	0.108
Ultra 3.8	2.5 to 3	0 to 0.1	4 to 6	angled	perc50to75	98.348	1.525	0.127
Ultra 3.8	2.5 to 3	0 to 0.1	4 to 6	angled	perc75to100	99.764	0.118	0.118
Ultra 3.8	2.5 to 3	0 to 0.1	4 to 6	angled	fullyBuried	99.353	0.324	0.324
Ultra 3.8	2.5 to 3	0 to 0.1	4 to 6	perpendicular	lessthan20percent	0.118	50.412	49.47
Ultra 3.8	2.5 to 3	0 to 0.1	4 to 6	perpendicular	perc20to50	38.023	61.905	0.0722
Ultra 3.8	2.5 to 3	0 to 0.1	4 to 6	perpendicular	perc50to75	98.667	1.244	0.0889
Ultra 3.8	2.5 to 3	0 to 0.1	4 to 6	perpendicular	perc75to100	99.831	0.0847	0.0847
Ultra 3.8	2.5 to 3	0 to 0.1	4 to 6	perpendicular	fullyBuried	99.581	0.21	0.21
Ultra 3.8	2.5 to 3	0 to 0.1	6 to 9	parallel	lessthan20percent	0.334	13.712	85.953
Ultra 3.8	2.5 to 3	0 to 0.1	6 to 9	parallel	perc20to50	6.796	90.291	2.913
Ultra 3.8	2.5 to 3	0 to 0.1	6 to 9	parallel	perc50to75	75.871	23.881	0.249
Ultra 3.8	2.5 to 3	0 to 0.1	6 to 9	parallel	perc75to100	99.219	0.521	0.26
Ultra 3.8	2.5 to 3	0 to 0.1	6 to 9	parallel	fullyBuried	98.83	0.585	0.585

Appendix D: List of Scientific and Technical Publications from MR-2227

Brandt, A., S.E. Rennie, 2013. "UXO Mobility – Initial Laboratory Test Series", Johns Hopkins University Applied Physics Laboratory Technical Memorandum KTF-13-072, Laurel, MD, 28 August 2013.

Rennie, S., and A. Brandt, 2014. "Probabilistic Modeling of Object Migration in the Coastal Zone", Poster # 1084, AGU/ASLO/TOS Ocean Sciences 2014, Honolulu, Feb 23-28, 2014.

Rennie, S. E., Brandt, A., 2014. "Underwater Munitions Expert System to Predict Mobility and Burial: Domain Knowledge Extraction," Johns Hopkins University Applied Physics Laboratory Technical Memorandum FPS-T-14-0179, Laurel, MD, April 2014.

Rennie, S.E., A. Brandt, 2014. "Experimental Determination of Underwater Munitions Mobility and Burial," Johns Hopkins University Applied Physics Laboratory Technical Memorandum FPS-T-14-0575, Laurel, MD, December 2014.

Rennie, S.E., A. Brandt, 2015. "Underwater Munitions Expert System: Preliminary Design Report," Johns Hopkins University Applied Physics Laboratory Technical Memorandum FPS-T-15-0333, Laurel, MD, August 2015.

Friedrichs, C.T., S.E. Rennie, A. Brandt, 2016. "Self-burial of objects on sandy beds by scour: A synthesis of observations," J.M. Harris, R.J.S. Whitehouse, S. Moxon (eds.), Scour and Erosion. CRC Press. 179-189.

Rennie, S.E., A. Brandt, C.T. Friedrichs, 2017. "Initiation of motion and scour burial of objects underwater," *Ocean Engineering*, Vol 131, 282-294.